

## Article

# Numerical and Statistical Evaluation of the Performance of Carbon Fiber-Reinforced Polymers as Tunnel Lining Reinforcement during Subway Operation

Ishola Valere Loic Chango  and Jun Chen \*

School of Civil Engineering, Tongji University, Shanghai 200092, China

\* Correspondence: cejchen@tongji.edu.cn

**Abstract:** Ground vibrations during train operations have become a serious problem in recent years. Local residents often feel disturbed by the vibrations emanating from the railroad line. This inconvenience is particularly pronounced in loose areas traversed by subways. However, improving the mechanical properties of tunnels has been the subject of several studies. Among these works, the widely discussed fiber-reinforced polymer (FRP) is considered as a material that can be incorporated into the tunnel structure to increase stiffness, durability, and corrosion resistance. However, the function of FRP in the interaction between the soil and the tunnel during operation has scarcely been studied. In this study, the effectiveness of carbon fiber-reinforced polymers (CFRP) as reinforcement of tunnel lining on ground vibration is investigated. For this purpose, a nonlinear 3D finite element model was developed based on a subway section in Shanghai to simulate the dynamic behavior of the system. The moving subway load was modeled as a transient dynamic load via a DLOAD subroutine, in which the rail irregularities are taken into account. The numerical model was efficiently validated by field tests. Then, the efficiency of using CFRP as concrete reinforcement of the tunnel lining during the subway operation was investigated. In addition, a statistical analysis of the ground dynamic response depending on the CFRP bars properties is presented, evaluated, and discussed.

**Keywords:** ground vibration; tunnel; subway train; carbon fiber-reinforced polymer; 3D finite element model



**Citation:** Chango, I.V.L.; Chen, J. Numerical and Statistical Evaluation of the Performance of Carbon Fiber-Reinforced Polymers as Tunnel Lining Reinforcement during Subway Operation. *Buildings* **2022**, *12*, 1913. <https://doi.org/10.3390/buildings12111913>

Academic Editors: Jan Fořt and Elena Ferretti

Received: 2 October 2022

Accepted: 31 October 2022

Published: 7 November 2022

**Publisher's Note:** MDPI stays neutral with regard to jurisdictional claims in published maps and institutional affiliations.



**Copyright:** © 2022 by the authors. Licensee MDPI, Basel, Switzerland. This article is an open access article distributed under the terms and conditions of the Creative Commons Attribution (CC BY) license (<https://creativecommons.org/licenses/by/4.0/>).

## 1. Introduction

In recent years, the increasing modernization of cities has led to a general awareness of the serious effects of traffic-induced vibrations on the environment and urban life [1]. In all major cities of the world, the demand for subway transportation is increasing, which brings a major environmental problem related to the vibrations caused by subway operations [2,3]. The effects of vibrations caused by subways mainly affect the surrounding buildings, which are at risk of collapse if they become obsolete. In addition to the risk of affecting sensitive equipment in industry and research, vibrations affect people's work and health [4]. Exposure of the human body to indoor vibrations is evaluated in a certain range, which corresponds to the same range of vibrations caused by the subway [5]. Since the ground vibration and structure-borne noise caused by trains can be disturbing to humans, many countermeasures have been developed to reduce the effects of railroad vibration. Various types of isolation, such as open and filled trenches, concrete walls or piles, and flexible gas cushions, have been used [6].

Recently, due to unforeseen geological conditions leading to aging and deterioration of the structure [7,8], a new tunnel design based on fiber application has become one of the most important and promising technologies [9,10]. FRP was first used in the automotive, marine, and aerospace industries as a lightweight, high-strength, and high-modulus material [11]. With the advancement of technology, FRPs have become an attractive alternative for reinforcing concrete structures due to their advantages [12]. The performance of FRP

grids embedded in PCM-shotcrete was estimated by numerical analysis considering various factors, such as soil classes, degree of deterioration of the lining, and condition of the tunnel [10,13]. The experimental study conducted on a pre-damaged tunnel showed that the use of carbon fiber-reinforced polymers (CFRP) mesh as reinforcement improved the bearing capacity and stiffness of the tunnel [14]. In some countries, FRP as internal reinforcement, such as bars, has been developed to reinforce non-prestressed and prestressed concrete structures, and the overall level of research, demonstration, and commercialization has increased significantly [15–17]. Strengthening tunnel linings with FRP bars increases the strength and ductility of the structure and reduces the width of cracks [18]. Several methods for reliable reinforcement design have been developed to optimize the use of FRP reinforcement bars in tunnel linings [19–21]. A blast test on a tunnel vault showed that FRP steel bars can prevent the occurrence of cracks in concrete to some extent [22].

Several studies have looked at FRP-reinforced structures. Most of these studies are based on the behavior or ability of FRP to reinforce concrete and resist corrosion through laboratory experiments or numerical modeling. Other studies have focused on design methods to optimize FRP-reinforced concrete structures. However, there are very few, if any, studies that focus on the real objective: Investigating the role of FRP on the behavior of the entire system; namely, the actual impact of FRP as bunker reinforcement during an explosion or to improve the dynamic response of the soil during subway operation. Since FRP is a material that is likely to be used permanently in structures, it would be imperative to study in detail the actual effects of FRP in an operational structure. In this way, the function of FRP could be better evaluated to prevent damage.

### *Objectives*

The main objective of this study is to evaluate the effectiveness of FRP bars as reinforcement of tunnel lining in the presence of ground vibrations during subway operation. Then, the main factors that may affect the performance of FRP bars in improving dynamic ground behavior are evaluated. For this purpose, carbon fiber-reinforced polymers (CFRP) were selected for tunnel concrete reinforcement due to their high corrosion and chemical resistance, low density, high fatigue strength, and high elastic modulus [23,24]. In this context, a nonlinear 3D FE model of a double tunnel system was created using the Abaqus program [25]. The wheel load of the subway train was designed as a transient dynamic load implemented by a user-defined Fortran subroutine. For a more accurate characterization of the dynamic behavior of the tunnel lining, the plasticity behavior during concrete damage was included in the concrete properties. The reliability of the FE model was confirmed by comparing the calculated results with the vibration accelerations measured on the tunnel wall and the ground surface of the Shanghai subway line.

Subsequently, the influence of the CFRP bar reinforcement on the ground vibration was investigated. Statistical analysis was also performed to investigate the relationship between the distribution of ground vibration and the influencing factors, such as the type of CFRP, the CFRP bar used, and the location of the calculation point, as well as the effects of the interaction between the factors. The measured values were then recorded according to an orthogonal factorial matrix of the full fractional size L27 ( $3^{13-10}$ ). The orthogonal matrix L27 ( $3^{13-10}$ ) is a full fractional factorial design in which there are 13 columns that can be used to assign test factors and their interaction. In this case, with three factors and three levels, the total number of tests to be performed is  $3^3 = 27$ . Therefore, analysis of variance was applied to investigate the influence of each factor and its interaction on the ground vibrations.

## 2. The Three-Dimensional Finite Element Model of the Investigated Double Metro Tunnel

### 2.1. Numerical Model Description

#### 2.1.1. Concepts of Rail Track Dynamic Analysis

The wheelset loads of a moving subway train moving over the tracks at different speeds are undeniably dynamic. Therefore, the contact stress and the position of the axle loads are time dependent and can be considered as the sum of the static load and a constantly changing load. Various factors, such as the unevenness of the rail surface, the speed of the subway train, the weight, and the suspension system can affect the constantly changing dynamic load. The oscillating motion of the subway train due to the suspension system of the cars causes the dynamic axle loads to fluctuate by their average amplitudes during subway operation.

According to the usual FE procedure [26,27], the main equation of a nonconservative dynamical system with material damping can be defined by Equation (1). This mathematical statement can be solved by the implicit or explicit integration method in Abaqus. In this study, the implicit direct integration method is adopted since it is more efficient at the frequencies observed in the simulation of systems subjected to a moving load [28].

$$[M]\{\ddot{u}\} + [C]\{\dot{u}\} + [K]\{u\} = F(t) \quad (1)$$

where  $[M]$  represents the mass matrix;  $[C]$  represents the damping matrix;  $[K]$  represents the stiffness matrix;  $\{\dot{u}\}$  represents the velocity vector;  $\{\ddot{u}\}$  represents the acceleration related to nodes;  $\{u\}$  represents the displacement vector; and  $F(t)$  represents the external force vector related to the structural dynamic system.

#### 2.1.2. Subway Structure Model Geometry and Element Mesh

Shanghai Metro Line 8 (China) was selected as a reference to analyze the dynamic behavior of a structure at the intersection of two trains. The 44.1 km Shanghai Metro Line 8 starts at Shiguang Road in Yangpu District and ends at Shendu Highway in Minhang. The line consists of various route profiles, including tunnels and bridges. According to the objective, this study focused on the Shanghai Hongkou District Youth Sports Center-Xinghua Community section, which is defined by a double tunnel with a burial depth of 9 to 15 m.

The three-dimensional FE model, implemented in Abaqus, is 260 m long, 120 m wide, and 50 m high. The tunnel was built with a layered lining of segmental walls. The track system consists of rails, track slabs, and the track bed. As shown in Figure 1, the two tunnels are located at a depth of 11.1 m and have a spacing of 12.4 m, with the outer diameter of the tunnel lining being 6.2 m in each case. The soil in which the tunnel is buried consists of several partial layers corresponding to the Shanghai soil. The Euler-Bernoulli beam element was used to model the rail. A bond connection was used to ensure the mutual contact between the layers under the track slab with the continuity of the deformation of the interface [29]. A Cartesian coordinate system was used in which the transverse direction of the rail is indicated by the X-axis, the vertical downward direction by the Y-axis, and the longitudinal direction (direction of travel of the subway train) by the Z-axis.

When analyzing FE, the consistency of the mesh size has some influence on the analysis result. Meshing should be conducted to obtain the most accurate results. Several researchers have investigated the appropriate mesh size for a dynamic model. In [30], it was suggested that 20 mm should be used as the mesh length in the flow direction and between 15 and 18 mm in the lateral direction in the loading region. In the present study, the meshing of the FE model was carried out to increase the accuracy of the model. A relatively fine mesh was used along the path of the wheels since the stresses and displacements were high. A dense mesh was used near the loading area, while a relatively coarse mesh was used outside the loading area (Figure 2). The depth of the 3D mesh in the model was chosen appropriately depending on the thickness of each layer to avoid errors and

warnings related to the mesh during the analysis. To improve the convergence rate, a continuum 3D-reduced-integration element (C3D8R) with eight nodes was used in the finite element field, while a continuum 3D infinite integration element (CIN3D8R) with eight nodes was chosen to define infinite boundaries on each side of the model of the tunnel system (Figure 2) [31].

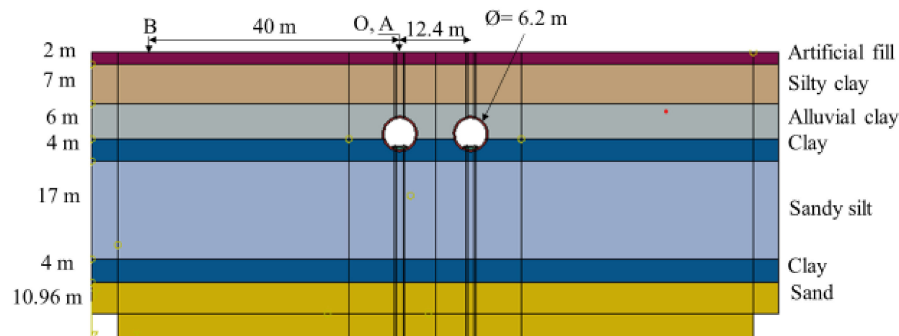


Figure 1. Tunnel description.

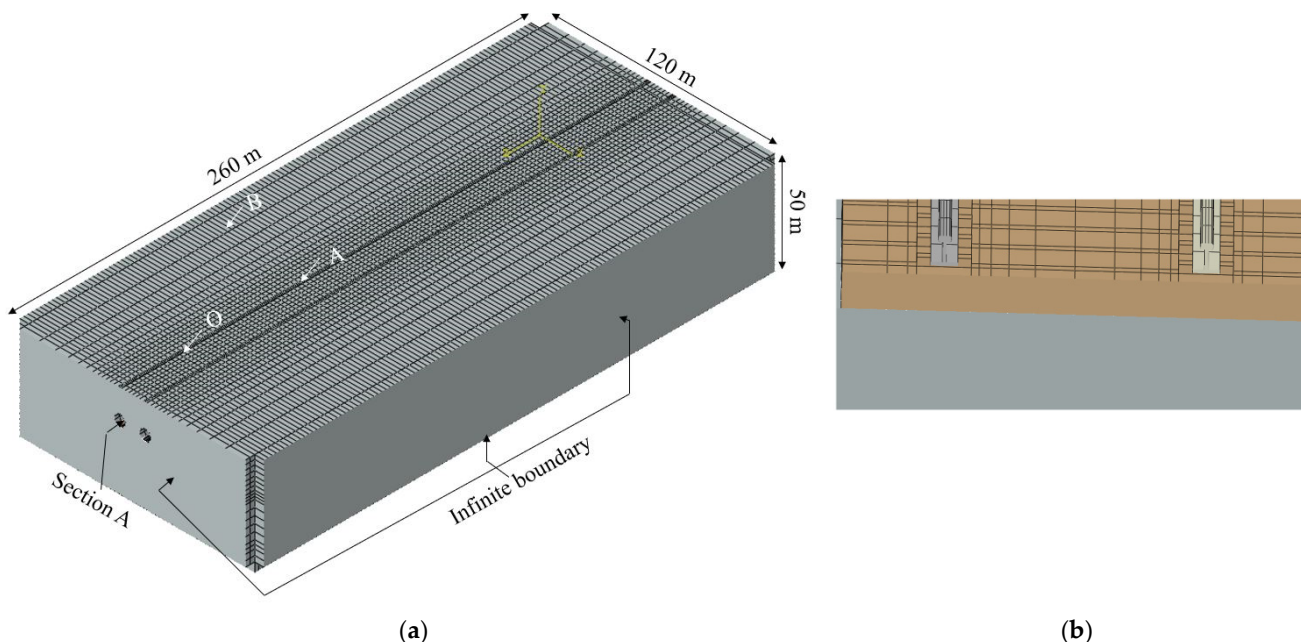


Figure 2. Model 3D mesh. (a) Mesh and boundary conditions view; (b) section A.

### 2.1.3. Boundary Condition and Material Damping

The boundary conditions imposed had some influence on the accuracy of the FE analysis results, thus it was important to choose appropriate and adequate boundary conditions. The boundary of a FE model is usually artificial; the wave generated by a moving subway train may propagate in the area of the structure until it is reflected at the artificial boundary, eventually contaminating the propagation of the wave in the domain. Therefore, previous studies have recommended the construction of non-reflecting or absorbing boundaries. As a result, an infinite element was chosen to eliminate the boundary effect of the tunnel model, absorb the wave energy, and reduce the degree of freedom in the far field. These elements are known to produce a quiet boundary without significant loss of precision for dynamic analyses [32].

The damping mechanism is a factor that affects the dynamic behavior of materials. It is related to the system itself, the viscosity of the surrounding medium, the energy dissipation of the subsurface, etc. Due to its complexity, it is difficult to accurately determine the damping matrix in FE analysis. The stress-energy factor method, modal damping method,

stiffness factor method, and Rayleigh damping method are used to calculate the damping. In this FE analysis, the Rayleigh damping method was used, assuming that the damping matrix is a linear combination of the mass matrix and the stiffness damping proportion. The corresponding equation is defined in Equation (2).

$$C = \alpha[M] + \beta[K] \quad (2)$$

where  $\alpha$  represents the mass damping coefficient; and  $\beta$  represents the stiffness damping coefficient. Therefore, the damping coefficients  $\alpha$  and  $\beta$  depending on the structural natural frequency are assessed following Equation (3).

$$2\omega\xi = \alpha + \beta\omega^2 \quad (3)$$

With

$$\begin{cases} \alpha = 2\omega_1\omega_2 \frac{\omega_1\xi - \omega_2\xi}{\omega_1^2 - \omega_2^2} \\ \beta = 2 \frac{\omega_1\xi - \omega_2\xi}{\omega_1^2 - \omega_2^2} \end{cases} \quad (4)$$

The computational process of Rayleigh damping parameters is determined by a modal analysis performed with the numerical model implemented in Abaqus. The 50 natural frequencies were extracted (Table A1) to determine the natural angular frequency  $\omega$  ( $\omega = 2\pi f$ ). Therefore, the natural angular frequency  $\omega_1$  was determined by defining the fundamental natural frequency  $f_1$ . After defining the fundamental frequency, the second angular frequency  $\omega_2$  was determined based on the highest natural frequency selected from the other order vibration modes. It follows that the natural angular frequencies  $\omega_1$  and  $\omega_2$  determined for the calculation of the Rayleigh damping parameters are 17.31 and 19.89 rad/s, respectively. In this study, the damping rate  $\xi$  for the structure was chosen between 2% and 4%. With damping rate  $\xi$  between 2% and 4%, the Rayleigh damping coefficients  $\alpha$  and  $\beta$  of the structure were calculated using Equation (4). The proportional damping value  $\alpha$  is 0.69529 and the stiffness proportional damping value  $\beta$  is 0.0032.

## 2.2. Track Materials Characterization and Soil Profile

Assuming an elastic layer system, all railroad materials are linearly elastic. The rubber pads and the fasteners between the slab and the rail are considered as linear elastic components and were modeled using spring-damper elements with a damping coefficient of 45 kN s/m and a stiffness value of 45 kN/mm [33]. The material properties of the track and the specification values were taken from the results of previous work and are listed in Table 1.

Following some previous experiments [34,35], a soil profile corresponding to the typical conditions for soft soils in the Shanghai region was selected for this study. The soil profile studied at a depth of 100 m rests on an underlying rigid soil with an average shear wave velocity of 500 m/s. The rigid soil, which is at a greater depth, was not considered in this study to shorten the simulation time. In this way, the infinite boundary condition was applied below the last soil layer, as shown in Figure 2. The variation of shear wave velocities, density, cohesion  $C$ , and friction angle  $\varphi$  for the selected representative soil profile used for the numerical analysis is given in Table 1.

For the typical dynamic properties of Shanghai clay and sand, the variations of shear modulus  $G/G_{\max}$  and damping ratio  $D$  with shear strain level  $\gamma$  are shown in Figure 3, based on the results of numerous resonant columns and cyclic triaxial tests [36]. It is worth noting that the groundwater effect was not considered in the dynamic analysis of the soil system. The shear modulus at low strain of the soil profile was derived from the dynamic properties as follows:

$$G_{\max} = \rho V_s^2 \quad (5)$$

where  $G_{\max}$  represents the ground small strain-shear modulus,  $V_s$  represents the ground shear wave velocity, and  $\rho$  represents the ground density.

Table 1. Mechanical properties of the ground layers.

Materials Designation	Unit Weight (KN/m <sup>3</sup> )	Initial Void Ratio	Compression Modulus (MPa)	Poisson Ratio	Cohesion under CU Test (kPa)	Friction Angle under CU Test (°)	Permeability Coefficient	Shear Velocity $t$ (m/s)
Rail	78	-	$210 \times 10^3$	0.3	-	-	-	-
Track slab	25	-	$32.4 \times 10^3$	0.2	-	-	-	-
				Soil type				
Artificial fill	17.8	0.96	5	0.33	10	13		110
Silty clay	18.6	0.86	9	0.32	14	12.5	$1 \times 10^{-7}$	130
Alluvial clay	16.9	0.92	2.12	0.35	12	10.5	$4 \times 10^{-8}$	140
Clay	17.5	0.82	3.13	0.33	16	12	$2 \times 10^{-7}$	160
Sandy silt	18	0.78	5.44	0.28	12	18	$8 \times 10^{-7}$	190
Sand	18.7	0.68	12.82	0.26	4	30	$5 \times 10^{-5}$	250

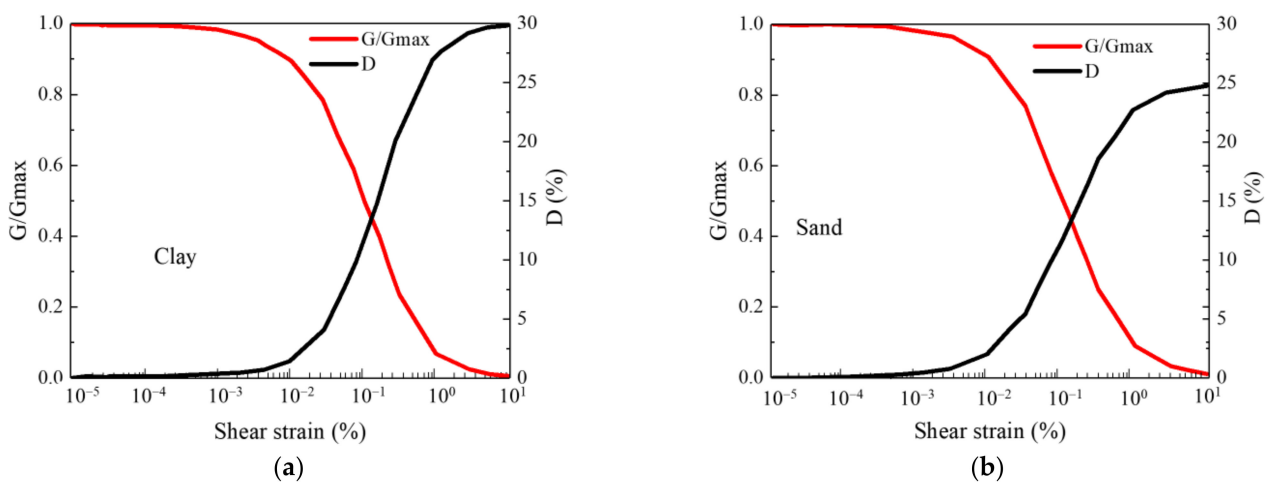


**Figure 3.** Typical  $G$ - $\gamma$ - $D$  curves for Shanghai soils. (a) Clays; (b) loose sands.

### 2.3. Characteristics of the Tunnel Structure

The tunnels of the Shanghai metro system are mainly constructed using the shield tunnelling method with a typical single-tube structure, i.e., a circular tunnel and a double-tube tunnel (DOT) with burial depths ranging from 9 to 33 m (Figure 4) [37]. The present work focuses on the dynamic response of the soil when a subway train passes through a subway tunnel. The subway studied here is a double tunnel with a typical circular cross-section. The two tunnels, which are 12.4 m apart and have an outer diameter of 6.2 m, were excavated using the shield tunnelling method, similar to the majority of tunnels in Shanghai. Therefore, after the tunnel was driven, the first lining (primary support) was made of steel ribs and fiber-reinforced shotcrete. Subsequently, the invert of the final lining was cast in plain concrete C35 with a thickness of 0.35 m.

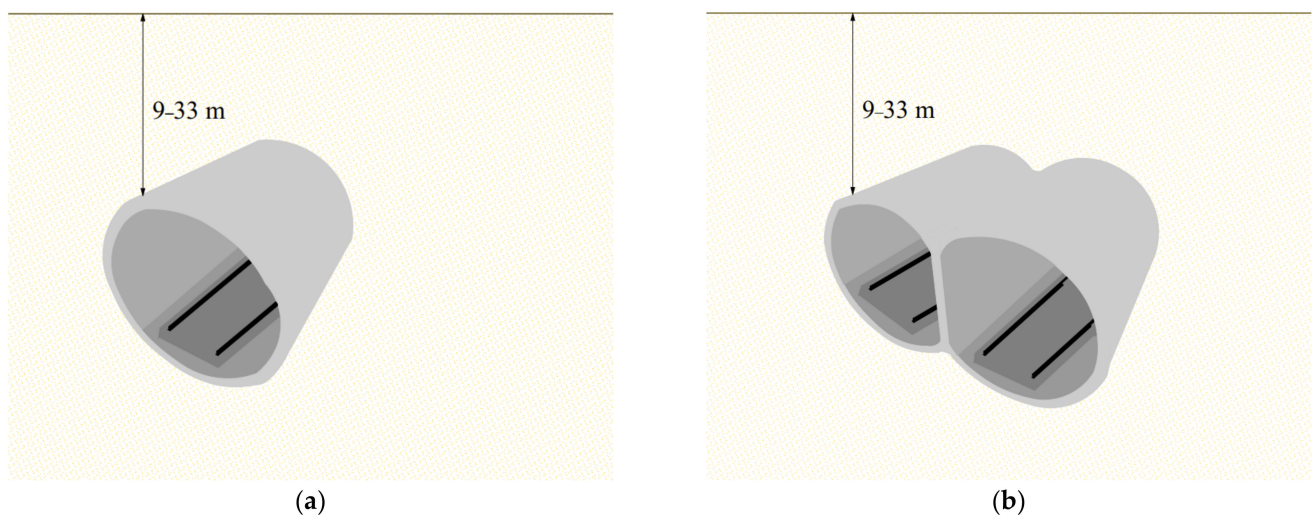


**Figure 4.** Type of tunnel often adopted in Shanghai. (a) Circular tunnel; (b) double-tube tunnel (DOT).

This study focuses on the effects of the final lining of the tunnel, which serves as a protective shield in the propagation of vibrations in the soil. Therefore, the resistive contribution of the first stage lining was neglected to reduce the simulation time due to the size of the 3D model. Moreover, this is a commonly accepted hypothesis since the stiffness of the shotcrete outer shell, which is in direct contact with the soil, is often neglected due to the fact that it may have undergone a physicochemical reaction that alters its original mechanical properties [38]. The geometrical and mechanical properties of the investigated tunnel sections are listed in Table 2.

**Table 2.** Physical parameters of the studied tunnel lining.

Density (g/cm <sup>3</sup> )	Elastic Modulus (GPa)	Poisson Ratio	Dilatation Angle (°)	Viscosity Parameter	Eccentricity	K
2.4	3.55	0.2	35	0	0.1	0.67

Concrete damage plasticity “CDP” is one of the most popular concrete models used to simulate concrete behavior in Abaqus. For a complete definition of the CDP model in Abaqus, the following mandatory parameters should be entered:  $f_{b0}/f_{c0}$ , a ratio between the compressive strength in the biaxial state and the compressive strength in the uniaxial state, which is set to 1.16 as the default value in Abaqus, and the ratio K of the second stress invariant on the tensile meridian to the compressive meridian for the yield function, the dilatation angle, and the viscosity parameter [39].

#### 2.4. Subway Dynamic Load Model

A six-car type A subway train manufactured by CNR Changchun Railway Vehicles Co., Changchun, China, was used for the field tests (Table 3). The individual components of the subway cars are considered as rigid parts connected by damper-spring elements. In this study, it was assumed that each subway car is properly proportioned and can be divided into four parts. The connection of the different car parts is shown in Figure 5. To specify the non-uniform distributed subway train load (DLOAD), the dynamic force due to the car movement on the rail was developed as a transient local dynamic load via a subroutine that allows the user to specify the magnitude change in the distributed load as a time functional form (TIME \*), coordinates (COORDS \*), the number of load integration points applied, and the number of domain elements [40]. The simplification of the calculation methods has led to the assumption that the wheels of the subway and the rails are always in contact, which indicates that there is no relative vertical displacement during the operation.

**Table 3.** Metro-train parameters of type A subway.

Mass of carriage (kg)	50,878	Inertia of Bogie/(kg·m <sup>2</sup> )	3605
Mass of Bogie (kg)	2721	Stiffness of primary suspension spring (N/m)	$2.14 \times 10^6$
Mass of Wheel Axle (kg)	1900	Damping of primary suspension spring (N·s/m)	$4.9 \times 10^4$
Inertia of Carriage/(kg·m <sup>2</sup> )	$2.446 \times 10^6$	Stiffness of secondary suspension spring (N/m)	$2.5 \times 10^6$
Distance of Wheel Axle in a Bogie (m)	2.50	Damping of primary suspension spring (N·s/m)	$1.96 \times 10^5$
Distance of Bogies in a Carriage (m)	15.7	Radius of Wheel/m	0.42

The irregularity of the rail is regularly modeled as a simple or composite concave cosine wave [41]. Therefore, the presence of a cosine track irregularity ( $Z_w$ ) on top of the rail is assumed with an amplitude A and wavenumber  $k_x$  (with  $\lambda$ , the wavelength). The track irregularity is defined as follows:

$$z_w(t) = A(1 - \cos(k_x t)) \quad (6)$$

The model of the subway train, which consists of six cars for the test, is created considering the quarter car model. Each car consists of two bogies with two sets of wheels

per bogie. The contact force between the car wheelset and the rail, defined in [42], was expressed as follows, taking into account the track irregularities:

$$p(y, t) = \sum_{n=1}^6 \sum_{i=1}^4 p_{ni}(y - vt) \quad (7)$$

where  $y$  is the distance between the subway-train axle and a reference point at the subway-train head;  $v$ ,  $t$ , and  $i$  are the metro-train speed, the time, and the axles numbering in a metro-carriage, respectively;  $p_{ni}(y - vt)$  is the  $i$ th subway-train wheels pair in the  $n$ th subway-train wheelset-rail contact force:

$$\begin{aligned} \sum_{i=1}^4 p_{ni}(y - vt) = & p_{n1}\delta\left(y - vt + \sum_{q=0}^{n-1} L_q + L_0\right) + p_{n2}\delta\left(y - vt + c_n + \sum_{s=0}^{n-1} L_q + L_0\right) \\ & + p_{n3}\delta\left(y - vt + c_n + d_n + \sum_{s=0}^{n-1} L_q + L_0\right) \\ & + p_{n4}\delta\left(y - vt + 2c_n + d_n + \sum_{s=0}^{n-1} L_q + L_0\right) \end{aligned} \quad (8)$$

where  $L_0$  is the distance between a reference point in the operating direction and the subway-train head;  $L_q$  is the  $(n - 1)$ th length of a subway-carriage;  $c_n$  and  $d_n$  are the distance between two subway-train wheel axles in the  $n$ th subway-carriage and the distance between two adjacent subway-train axles in  $n$ th carriage bogies;  $\delta$  represents a Dirac Delta function.

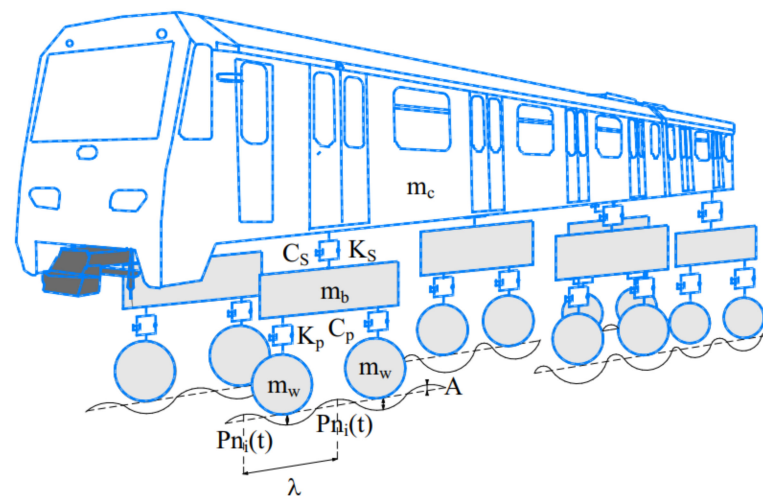


**Figure 5.** Metro-train geometry.

Substituting Equation (8) into the quarter-subway carriage model, the following expression was deduced:

$$P_{ni}(k_x, \omega) = W_{ni1}\delta(\omega - k_x v) + W_{ni2}\delta(\omega - \omega_r - k_x v) + W_{ni3}\delta(\omega + \omega_r - k_x v) \quad (9)$$

where  $\delta$  is a Dirac Delta function,  $W_{ni}$  represents the sub-item of the  $i$ th carriage wheel–rail contact force in the  $n$ th car, and  $\omega_r$  represents the excitation frequency due to rail surface irregularity, which can be defined by  $\omega_r = 2\pi v / \lambda$ ;  $\lambda$  is the rail wavelength.

The  $i$ -th transient dynamic of the subway wheel at a position  $x$ , obtained with Fortran and included in the implicit analysis, was defined by the combination of Equations (6) and (9). The equivalent parameters of the subway model are summarized in Table 3.

Depending on the type of section studied, two scenarios were considered, upward and downward. Therefore, the scenario where two subway trains run simultaneously in the upward and downward direction was also developed using the Fortran subroutine.

### 3. Numerical Model Validation

#### 3.1. Comparative Analysis between Numerical Model Result and Field Measurements

The validation of the model was conducted in two stages, which are described below.

##### Stage 1

In the first phase, field measurements were conducted on top of a subway tunnel in the section of Line 8 between the Shanghai Hongkou District Youth Sports Centre and Xinghua Community. During the vibration measurement campaign, several points were selected that were triggered by subway vehicles (see Figure 6). The accelerometers used are LPMS-B2 series sensors with a frequency range of 0 to 400 Hz, a measurable acceleration field of 0.1 to 10 g, a latency of 20 ms, an accuracy of  $<0.5^\circ$  (static) and  $<2^\circ$  RMS (dynamic), an operating voltage of 5.5 VDC, an output voltage range of 0.5 to 4.5 V, and an operating temperature of  $-40$  to  $80^\circ\text{C}$ .

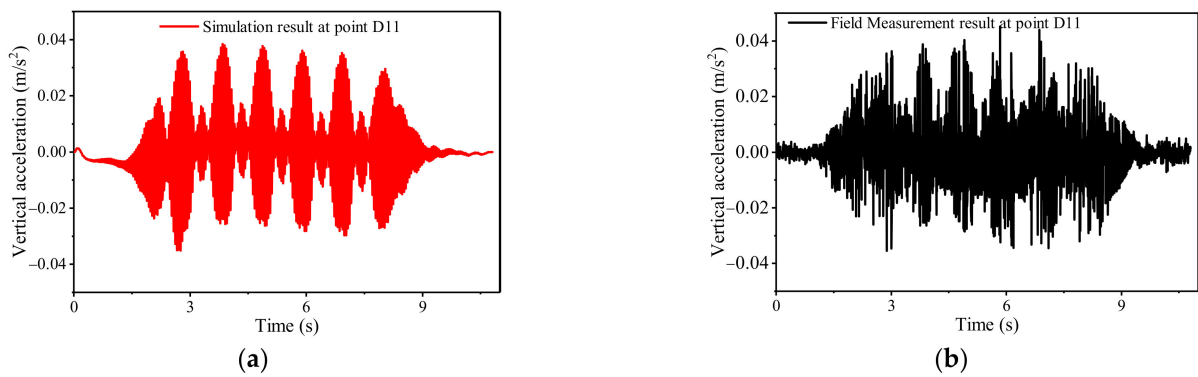


Figure 6. Distribution of monitoring point.

During the field measurement, the sensor frequency was set to 200 Hz while the metro train was traveling at approximately 80 km/h. Points D11 and D12 (see Figure 5) were selected for model validation due to their proximity to the tunnel. The other points were not considered due to their location, which could be influenced by external traffic.

The dynamic accelerations at points D11 and D12 (top of the ground) are shown in Figures 7 and 8. In both figures, the periodic occurrence of a wave crest series can be seen. The amplification of these waves in a given period corresponds to the dynamic effect of each subway bogie when it comes into contact with the respective location. Moreover, a great similarity was observed between the data measured in the field and the results calculated with the FE model. In Figure 7, the dynamic acceleration RMS measured in the field is  $1.15 \times 10^{-2} \text{ m/s}^2$  and the calculated dynamic acceleration RMS is  $1.24 \times 10^{-2} \text{ m/s}^2$ . The specified difference is 7.26% on average. In Figure 8, the dynamic acceleration RMS measured in the field was  $5.32 \times 10^{-3} \text{ m/s}^2$ , and the calculated dynamic acceleration RMS was  $4.79 \times 10^{-3} \text{ m/s}^2$ . Here, the reported difference is 9.96% on average.

In Figure 9a,b, the frequency spectrum at points D11 and D12 were depicted. In both figures, a great similarity was observed between the data measured in the field and the results calculated with the FE model. In Figure 9a, the acceleration amplitude RMS measured in the field is  $8.54 \times 10^{-4} \text{ m/s}^2/\text{Hz}$  and the calculated acceleration amplitude RMS is  $7.61 \times 10^{-4} \text{ m/s}^2/\text{Hz}$ . The specified difference is 10.88% on average. In Figure 9b, the acceleration amplitude RMS measured in the field was  $3.23 \times 10^{-4} \text{ m/s}^2/\text{Hz}$ , and the calculated acceleration amplitude RMS was  $2.87 \times 10^{-4} \text{ m/s}^2/\text{Hz}$ . Here, the reported difference is 11.14% on average.



**Figure 7.** Vertical acceleration at point D11. (a) Numerical model result; (b) Field measurement result.

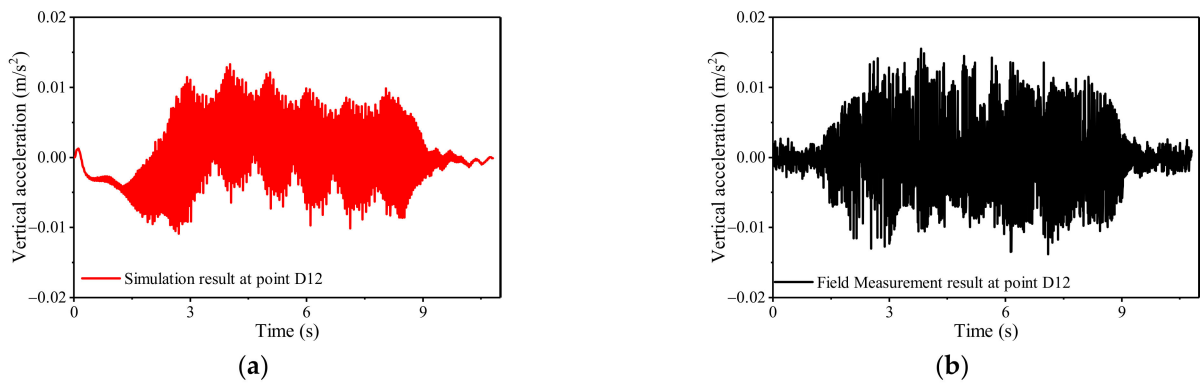


**Figure 8.** Vertical acceleration at point D12. (a) Numerical model result; (b) Field measurement result.

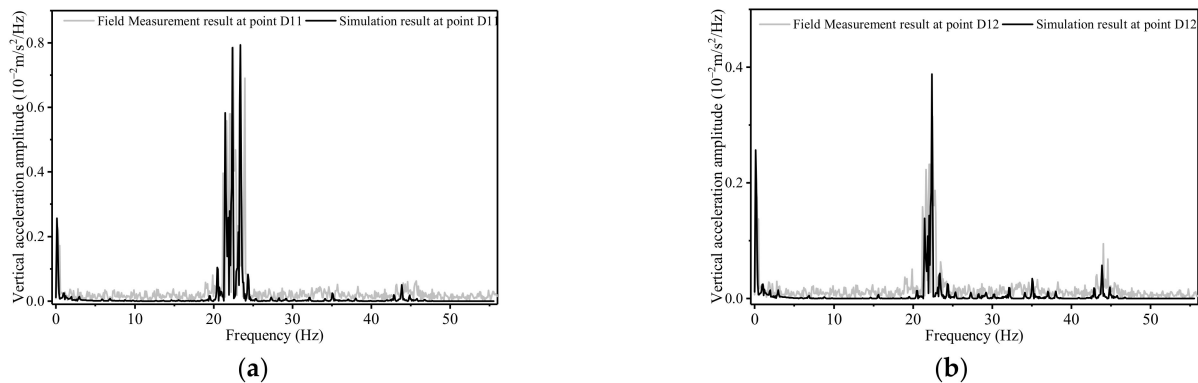


**Figure 9.** Vertical acceleration amplitude at points D11 and D12. (a) Numerical model result; (b) Field measurement result.

## Stage 2

This second stage of numerical model validation is based on the in situ measurement of the dynamic response of a double tunnel system in Shanghai presented by S. Zhou et al. [43]. At this stage, only the time history was considered, since this is the only data available from Zhou's work to verify the results of the numerical model in the context of this work. A six-car type A subway train is also used on this subway line, which passes through the test site at a speed of about 54 km/h. To record the accelerations induced by the subway train, two measurement points were placed on the tunnel cross section as shown in Figure 10.

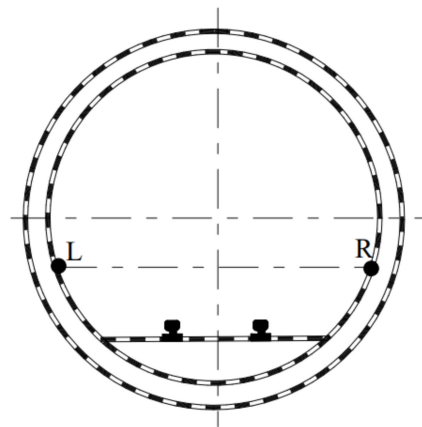


**Figure 10.** Schematic diagram of the measuring points in the tunnel.

The dynamic accelerations at points R and L are shown in Figures 11 and 12. In all figures, the periodic occurrence of a wave crest series can be seen. The amplification of these waves in a given period corresponds to the dynamic effect of each metro bogie when it is in contact with a given location. Moreover, a high agreement was observed between the data measured in the field and the results calculated with the FE model. In Figure 11, the maximum dynamic acceleration measured in the field is  $0.338 \text{ m/s}^2$  and the calculated maximum dynamic acceleration is  $0.366 \text{ m/s}^2$ . The specified difference is 7.65% on average. In Figure 12, the maximum dynamic acceleration measured in the field was  $0.341 \text{ m/s}^2$ , and the calculated maximum dynamic acceleration was  $0.360 \text{ m/s}^2$ . Here, the reported difference is 5.28% on average.

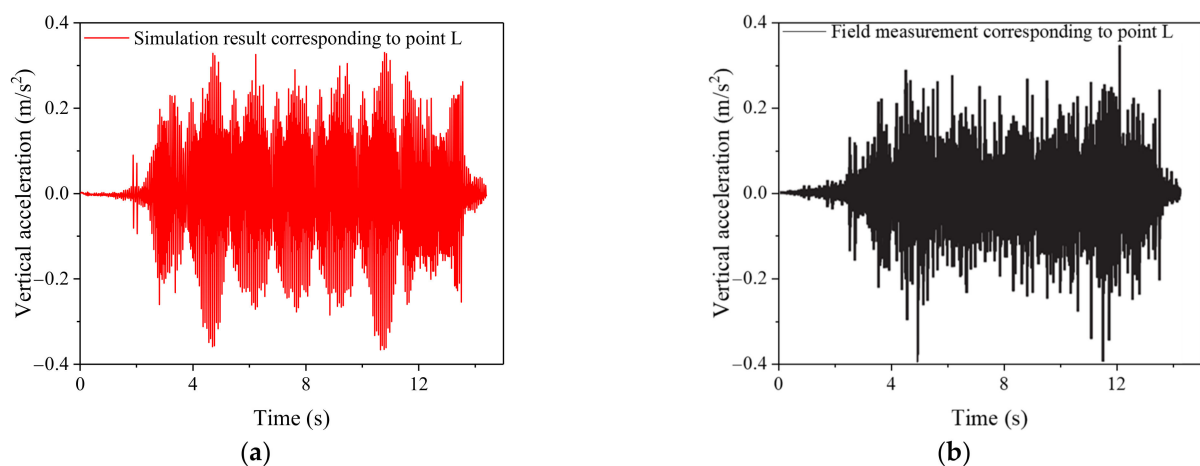


**Figure 11.** Vertical acceleration at point L. (a) Vertical acceleration from numerical model; (b) vertical acceleration from field test measurement Reprinted from Ref. [43]. 2019, Zhou Shunhua.

Combining the results observed in Stages 1 and 2, the causes of the observed differences could be due to some of the conditions described below:

- (1) The intended speed fluctuated since it was difficult to maintain the speed of the metro train as stable during the operation.
- (2) The sensors are subjected to vibrations when the subway train approaches and remain subjected to these vibrations even after the wheelset passes. As a result, the response of the sensors is affected. This illustrates the difference between the inclination of the spikes of the 3D FE model and the vibrations of the field measurement.
- (3) The controlled wheel forces of the subway train were assumed to be uniformly distributed over a contact area between each wheelset and the rails.
- (4) Rayleigh damping parameters are based on a modal analysis of the whole system, while in the field each material responds according to its damping.

(5) The external traffic may affect the recorded data slightly.

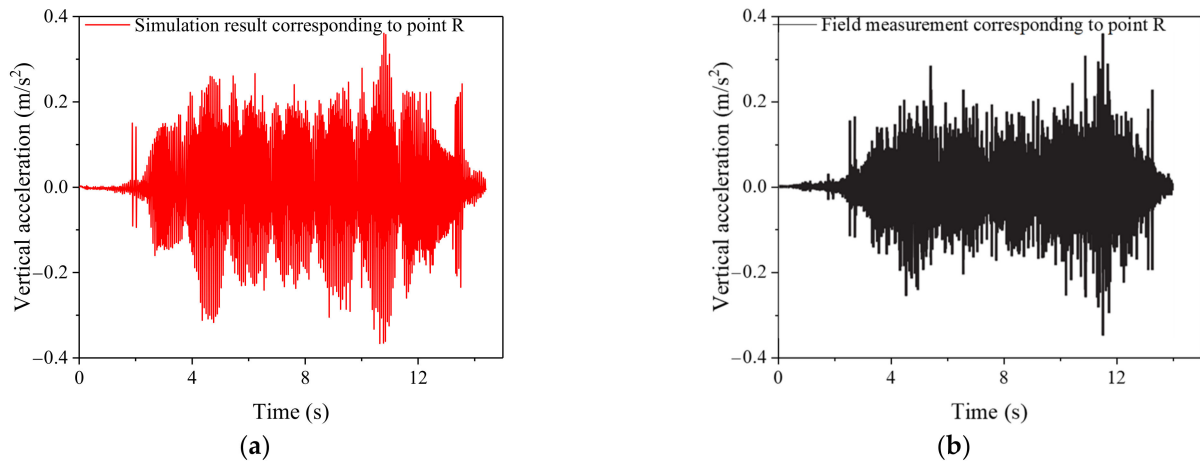


**Figure 12.** Vertical acceleration at point R. (a) Vertical acceleration from numerical model; (b) vertical acceleration from field test measurement Reprinted from Ref. [43]. 2019, Zhou Shunhua.

### 3.2. Correlation Analysis between the Numerical Results and Field Data Test

The comparative analysis between the field test data and the numerical results shows that the 3D FE model implemented in Abaqus accurately predicts the dynamic response of the metro system. Nevertheless, there is a slight margin of error in terms of the shape of the curve and the amplitude. To investigate the impact of these observed differences on the accuracy of the model in predicting the dynamic response of the structure, a correlation study was performed considering all variables. The measured vibration accelerations from the calculation with the numerical model and from the field tests were processed. The correlation between two variables  $u$  and  $v$  is obtained by calculating a coefficient  $\gamma_{uv}$ .

$$\gamma_{uv} = \frac{\sum(u_i - \bar{u})\sum(v_i - \bar{v})}{\sqrt{\sum(u_i - \bar{u})^2}\sqrt{\sum(v_i - \bar{v})^2}} \quad (10)$$

where  $\bar{u} = \frac{1}{n}\sum_i^N u_i$  denotes the mean of  $u$ ; and  $\bar{v} = \frac{1}{n}\sum_i^N v_i$  denotes the mean of  $v$ .

The calculation of the Pearson coefficient of correlation leads to a result in the interval  $(-1;1)$ ; the sign indicates the direction of the relationship. However,  $r = 0$  indicates that there is no linear relationship. The degree of correlation between the results calculated with the FE model and the measured field data is given in Table 4.

**Table 4.** Correlation matrix of field data and numerical model.

		FE Model				Sig (Two-Tailed)
		Vibration Acceleration at Point D11	Vibration Acceleration at Point D12	Vibration Acceleration at Point L	Vibration Acceleration at Point R	
Field Test	Vibration acceleration at point D11	0.985 **				0.000
	Vibration acceleration at point D12		0.991 **			0.000
	Vibration acceleration at point L			0.987 **		0.000
	Vibration acceleration at point R				0.982 **	0.000

\*\* : Correlation is significant at the 0.001 level (two-tailed).

The presentation of the correlation matrix of the vibration accelerations measured during the field tests and the results of the FE model shows that the correlation factor varies between 0.982 and 0.991 depending on the location. Therefore, the dynamic response of the metro system calculated by the FE model and the vibrations measured during the field test at different locations have a very significant correlation at the level of 0.001. As a result, the

difference between the results of the FE model and the field data in terms of the shape and magnitude of the curve does not affect the ability of the FE model to accurately predict the dynamic response of the subway system during the subway operation.

#### 4. Influence of Subway Operation Direction on the Ground Vibration

Since the purpose of this study is to analyze the environmental ground vibration caused by the moving subway train, it is important to study the unfavorable case to better evaluate the dynamic behavior and the different solutions to improve the dynamic behavior of the ground. During the subway operation, the crossing of two subway trains occurs frequently. During this overlapping period, a change in vibration is noticeable. In this section, the ground vibration is evaluated when the subway train travels in one direction and in two directions (upward and downward). The vibrations caused by the subway train were investigated in two cases. Case 1 is described by the operation of the subway train in a single upward direction at 60 km/h. Case 2 is described by the operation of two subway trains in upward and downward direction moving at the same speed of 60 km/h.

Figures 13 and 14 show the time history of the vertical acceleration and amplitude spectrum at the ground surface (point O) for both cases studied. This point was chosen to avoid a complete crossing of the two subway trains during the calculation by the numerical model. As can be seen, the time history of acceleration in case 1 differs significantly from case 2. More precisely, the maximum acceleration for case 1 and case 2 is  $0.417 \times 10^{-2} \text{ m/s}^2$  and  $2.313 \times 10^{-2} \text{ m/s}^2$ , respectively. The maximum acceleration for case 1, which is very small, is about 18% of the maximum acceleration for case 2. Moreover, the two amplitude spectral curves are similar in terms of the periodic occurrence of amplitude peaks in a certain frequency range of (0–3.75 Hz), (15.2–19.36 Hz), and (26.45–35.67 Hz). However, it should be noted that also in this section the maximum acceleration amplitude for case 1 is 21.6% of the maximum acceleration amplitude for case 2.

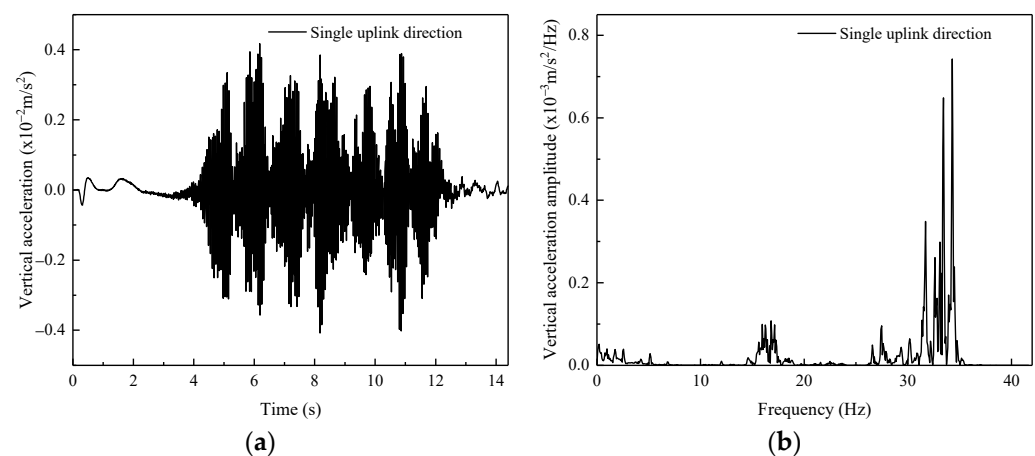


**Figure 13.** Vertical vibration at point O during the uplink operation. (a) Time history of dynamic acceleration; (b) acceleration amplitude-frequency.

From this analysis, it is clear that consideration of the ground vibrations caused by the two moving subway trains in the upward and downward directions is critical to evaluate the vibrations of the surrounding buildings and the effectiveness of the improvement methods. This analysis highlights the importance of considering the vibration effect caused by two trains traveling simultaneously in the upward and downward directions.

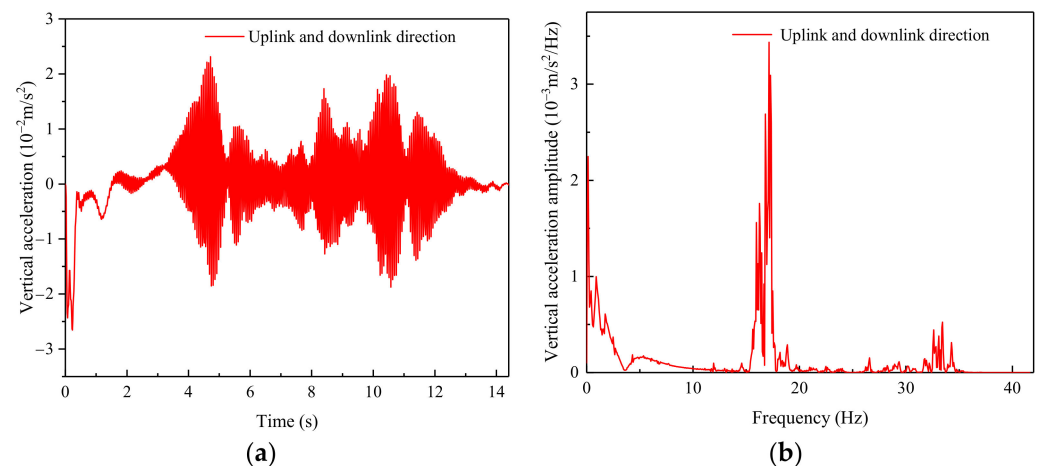


**Figure 14.** Vertical vibration at point O during the uplink and downlink operations. (a) Time history of dynamic acceleration; (b) acceleration amplitude-frequency.

## 5. Numerical Study of the Performance of the CFRP-Reinforced Tunnel

In this section, the effect of carbon fiber-reinforced polymers (CFRP) on the ground vibration caused by the moving subway train is investigated. In this case, the CFRP bars are used as reinforcement for the concrete of the tunnel lining.

### 5.1. Constitutive Model of CFRP Rebar-Reinforced Tunnel Lining Concrete

In typical applications, CFRP reinforcement consists of straight bars manufactured using a proven industrial pultrusion technology. In underground tunnels, reinforcement with a curved configuration is required, and the pultrusion process cannot be used. For this purpose, a modified pultrusion process called “forming” has been developed to produce curved bars with a constant and large radius of curvature. The behavior of prefabricated concrete segments with GFRP reinforcement produced by the tensile training technology is reported in [18,44]. In this study, the reinforcement cage consisted of continuous curved bars coupled in the longitudinal direction (intrados/extrados).

Starting from a traditional steel reinforcement cage (SR), which served as a reference, the CFRP reinforcement cage was designed in Abaqus. The reinforcement consists of curved bars of  $\text{Ø}12$  longitudinal frames with a spacing of 11 cm. The transverse reinforcement consists of  $\text{Ø}12$  bars of straight frames closed with stirrups spaced 11 cm apart, as shown in Figure 15. Elastic isotropic behavior to failure was assumed for the CFRP, which is considered a solid and homogeneous element. The Poisson’s ratio was assumed to be 0.3. The reinforcement cage was embedded in the tunnel lining with a concrete cover of 50 mm. The typical mechanical properties of the CFRP are given in Table 5. The high modulus polyacrylonitrile carbon was used for this study. The embedded element option was chosen to connect the CFRP reinforcement to the concrete. The reinforcement was used as the embedded two-noded deformable truss (T3D2R) element. It is assumed that the CFRP cage is well anchored to the concrete to act as an effective shear or tension reinforcement element.

### 5.2. Dynamic Behavior of Soil during Operation of Subways

In this section, the influence of CFRP on dynamic soil response is evaluated. For this purpose, the characteristic distribution of soil vibrations and the influence of subway train speed on CFRP performance are analyzed.

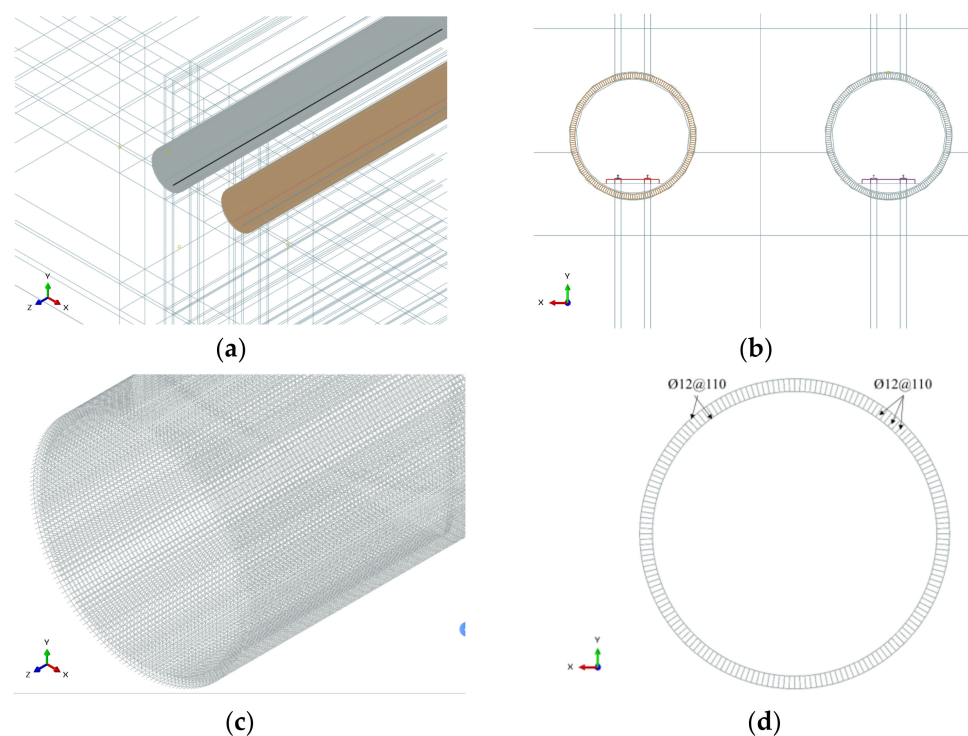


**Figure 15.** CFRP reinforcement cage model. (a) 3D view of the whole model with reinforcement; (b) 2D view of the model with reinforcement; (c) 3D view of the reinforcement cage model; (d) description of the rebar disposition.

**Table 5.** Typical mechanical property of carbon fiber-reinforced polymer (CFRP).

	Carbon Fiber			
	Polyacrylic Nitril Carbon		Pitch Carbon	
	High Strength	High Modulus	Ordinary	High Modulus
Density (kg/m <sup>3</sup> )	1.7–1.8	1.9	1.65	2.0
Tensile strength (MPa)	$3.4 \times 10^3$	$3.2 \times 10^3$	$0.9 \times 10^3$	$3.2 \times 10^3$
Young's modulus (GPa)	228	517	38	620.4
Elongation (%)	1.55	0.6	2.3	0.95
Coefficient of thermal expansion ( $10^{-6}/^{\circ}\text{C}$ )	−0.4	−0.65	−0.4	−0.8

### 5.2.1. Distribution Characteristics of Ground Vibrations Due to a Moving Subway Train

To represent the vibration characteristics caused by the subway train on the ground surface, a total of 4477 points are selected to evaluate the vibrations. The distance between two points follows the mesh lattice of the model, in order that two points located in the area of load application are very close to each other. The distance between two points increases the farther the points are from the load application area.

The color map of the ground vibrations in the time domain is obtained by linear interpolation, as shown in Figures 16 and 17. The vibrations at the top of the soil for the standard tunnel and the vibrations at the top of the soil for the structure reinforced with CFRP bars are shown in Figures 16 and 17, respectively. For both color plots, a large acceleration RMS (root-mean-square) is observed at the intersection of the two subway trains. The acceleration RMS decreases as the calculated point is close to the edges of the ground surface in the model. In Figure 16, three vibration amplified regions were observed in the crossing area of the two subway trains. Once the structure is reinforced with CFRP reinforcement (Figure 17), the vibration amplifications observed in the crossing area decrease. Moreover, when the tunnel structure is reinforced with CFRP reinforcement,

an average reduction of 6.4% in acceleration RMS is observed over the entire ground surface. However, it should be noted that the reduction rate varies from one point to another, as shown in Figure 18a.

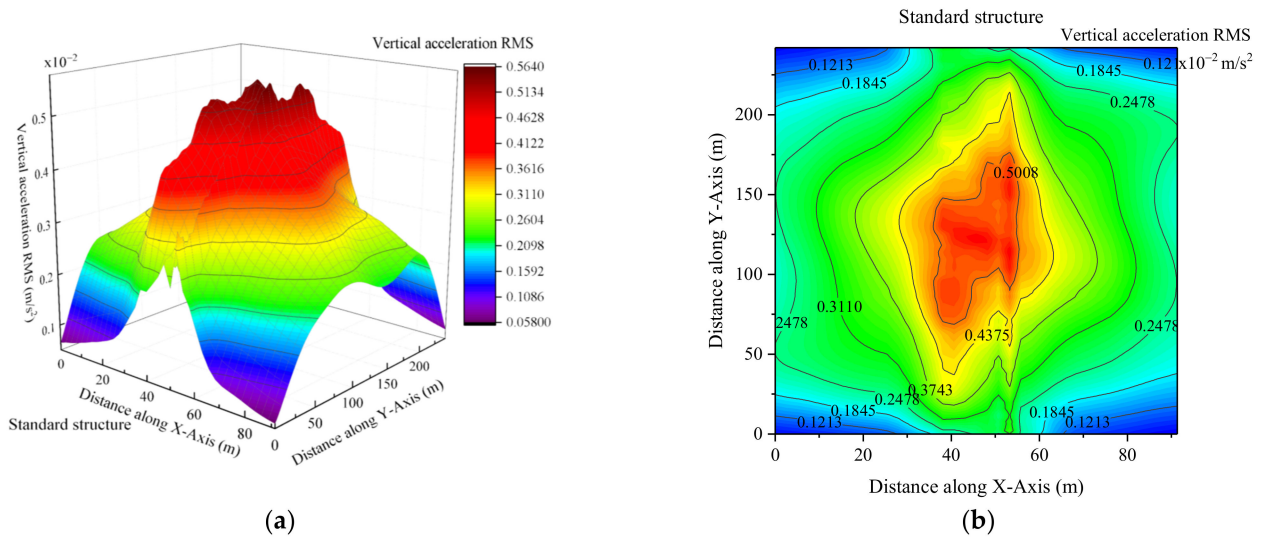


Figure 16. Color chart of the vibration RMS for the standard structure. (a) 3D diagram; (b) vertical view.

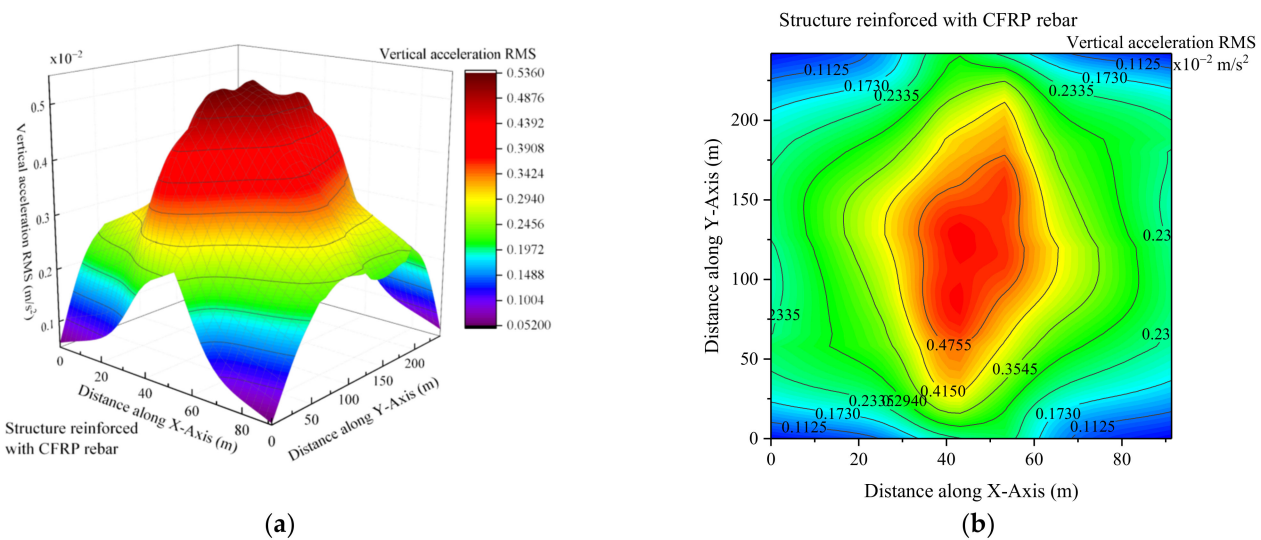
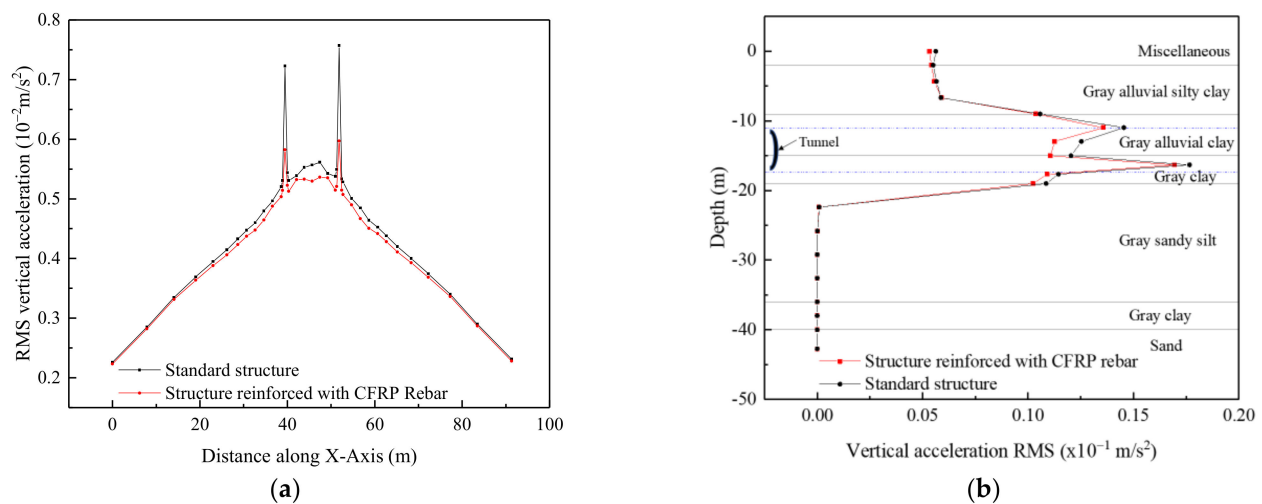


Figure 17. Color chart of the vibration RMS for the structure reinforced with CFRP rebar. (a) 3D diagram; (b) vertical view.

Figure 18a shows the calculated acceleration RMS along the X-axis, perpendicular to the subway train travel direction. As can be seen, the maximum calculated acceleration RMS are located above each tunnel’s center and decrease with the increasing distance. The calculation points corresponding to the two peaks are each located above the center line of each lane of the tunnel. Therefore, the combination of the effect of the two metro-train wheel lines located on either side of the track central line generates an increase in vibration at the track center of each tunnel. Therefore, vibration peaks are observed at the points above the center line of each tunnel track.



**Figure 18.** Vibration acceleration RMS. (a) Vibration RMS along model X-axis; (b) vibration RMS according to the depth.

For example, the acceleration RMS over the center (point A) of the standard tunnel and the tunnel reinforced with CFRP reinforcement is  $7.57 \times 10^{-3} \text{ m/s}^2$  and  $5.97 \times 10^{-3} \text{ m/s}^2$ , respectively. At the edge of the ground surface (point B, e.g., 0 m, as described in the graph), the acceleration for the standard tunnel and the tunnel reinforced with CFRP reinforcement is  $2.26 \times 10^{-3} \text{ m/s}^2$  and  $2.23 \times 10^{-3} \text{ m/s}^2$ , respectively. When the structure is reinforced with CFRP reinforcement, the acceleration RMS decreases by 21.14% above the center of the tunnel and by 6.63% on average in the area between the two tunnels. The reduction rate of the acceleration RMS varies from 3.89% to 1.33% as one moves away from the center of the tunnel.

The study of the distribution of acceleration RMS between the two tunnels as a function of depth is shown in Figure 18b. The acceleration RMS first increases with depth until it reaches a peak near the tunnel, then the acceleration RMS starts to decrease with the increasing depth. A peak was recorded at each pole line of the tunnel. In this case, amplified vibrations occur near the tunnel during subway operation. This phenomenon was also observed in the field measurement experiment by Qiang et al. [35]. When the tunnel lining is reinforced with CFRP reinforcement, a reduction in acceleration RMS in the soil is observed. The acceleration RMS is significant near the tunnel and decreases with the increasing or decreasing depth. The maximum acceleration RMS near the tunnel is  $1.77 \times 10^{-2} \text{ m/s}^2$  and  $1.69 \times 10^{-2} \text{ m/s}^2$  for the standard structure and the reinforced structure, respectively; which results in a reduced rate of 4.52%. Above the ground surface, the acceleration RMS reduction rate is about 5.51%.

Using  $\text{Ø}12$  CFRP rods to reinforce the concrete of the tunnel lining helps in reducing the vibration distribution caused by the subway train. The reduction rate varies from 1.33% to 21.14% at the top of the ground and 3.82% on average at the bottom, considering the depth at the center of the two tunnels.

Tunnels with plain concrete have been built all over the world taking into account the load that the tunnel will carry. This work shows that tunnel lining can also play a key role in the propagation of the induced vibration. Therefore, its design method has an impact on the vibrations in the system. This is due to the results obtained when the reinforcement is made with bars and, in particular, with fiber-reinforced composites (FRP) due to the many other advantages. For example, reinforcing the tunnel lining with CFRP bars increases the dynamic capacity of the soil to respond to the vibrations caused by the passage of a subway train in the tunnel. Therefore, the installation of CFRP bars in the tunnel structure improves the dynamic properties of the soil by reducing the vibration in the time domain during train operation. This phenomenon is an advantage for the foundations of the surrounding buildings, which are less affected by the various dynamic loads caused by the subway train.

### 5.2.2. The Influence of the Speed of the Metro Train on the Ground Vibrations Analysis at a Point Located on the Ground Surface above the Tunnel (Point A)

In this section, the frequency spectrum obtained with the fast Fourier transform is analyzed during subway operation. The objective of this analysis is, first, to investigate the dynamic behavior of the soil during subway train operation at different speeds in the tunnel and, second, to determine the effect of speed on the performance of the tunnel concrete reinforced with CFRP bars.

Figure 19 shows the acceleration spectrum at the ground surface above a tunnel centerline (point A). As can be seen, the number and size of the periodic amplitude cycles vary with speed. At 40 km/h, three periodic cycles are calculated with peak amplitudes averaging  $2.22 \times 10^{-1} \text{ m/s}^2/\text{Hz}$ . The number of significant periodic amplitude cycles decreases with the increasing speed with an increase in the maximum peak in the frequency domain. At 40 km/h, the subway train motion is considered quasi-static. Therefore, the relatively long time of wheel-rail contact generates low ground vibrations.

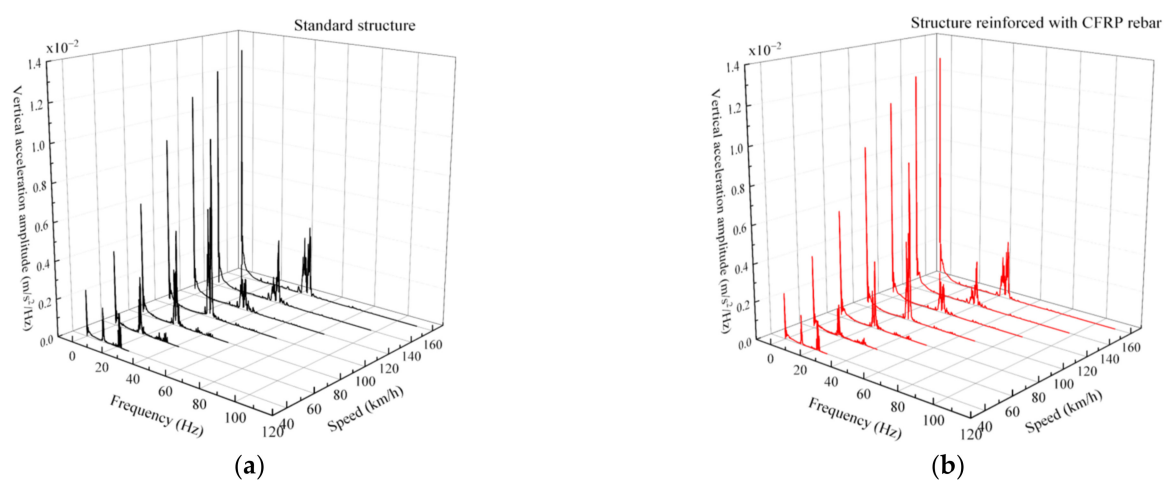


**Figure 19.** Spectrum of the vibration amplitude at point A. (a) Acceleration amplitude-frequency for the standard structure; (b) acceleration amplitude-frequency for the structure reinforced with CFRP rebars.

When the subway train reaches a speed of 100 km/h, the peak values of the second periodic series of acceleration amplitudes are larger than the peak values of the first periodic series of amplitudes; subsequently, the peak values of the second cycle of acceleration amplitude decrease with the increasing speed. This phenomenon can be attributed to the dynamic amplification in the frequency domain when the speed of the subway train reaches a certain value.

When the tunnel is reinforced with CFRP reinforcement bars, the acceleration amplitude at the ground surface above the tunnel centerline decreases regardless of the speed of the subway train. At a speed of 100 km/h, the value of the second cycle of acceleration amplitude peaks decreases significantly and becomes smaller than the peak value of the first periodic cycle of the amplitude. From this analysis, it appears that reinforcing the concrete of the tunnel lining with CFRP bars increases the stiffness of the ground-tunnel system, which would contribute to the gradual elimination of the vibrations amplified in the ground when the train reaches a certain speed.

Figure 20 shows the acceleration amplitude RMS at the ground surface at various subway speeds. As can be seen, dynamic amplification occurs in the frequency domain when the subway train reaches a speed of 100 km/h. It can be seen in Table 1 that this velocity coincides with the shear wave velocity of a soil layer. The influence of the concrete reinforcement of the tunnel lining with CFRP reinforcement bars on the ground vibrations varies from speed to speed. The reduction rate of the acceleration amplitude RMS increases with the increasing speed up to 100 km/h. At this speed, where amplification dynamics

in the frequency domain can be observed, the reduction rate of acceleration amplitude decreases, and then increases again with the increasing speed. Therefore, the reduction rate of vibrations at a subway speed of 40 and 80 km/h is 12.5% and 22.1%, respectively.

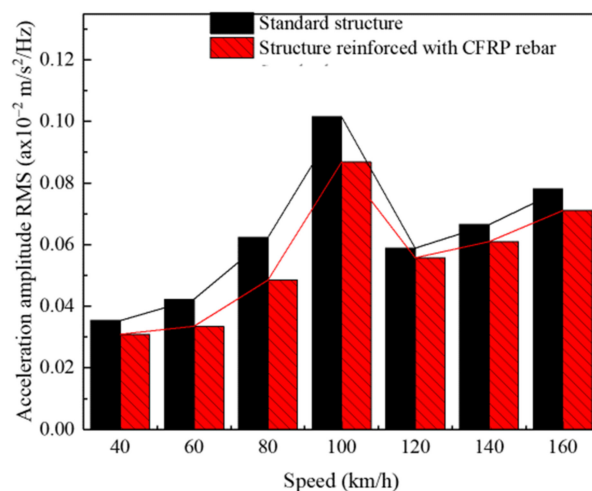


Figure 20. Acceleration amplitude RMS diagram at point A.

The installation of Ø12 CFRP bars in the concrete of the tunnel lining reduces the dynamic reinforcement to a certain extent. Using Ø12 CFRP bars helps in reducing the acceleration amplitude in the ground to a certain degree in order that the ground vibrations are less amplified when the speed changes from 80 to 120 km/h. This rate is determined by the gap between the acceleration amplitude RMS when the speed of the subway changes during operation, as described in Table 6. From this, it can be seen that the acceleration amplitudes RMS are close to each other when the structure is reinforced with CFRP bars. This value may vary depending on the type of CFRP used.

Table 6. Acceleration amplitude RMS at point A.

Speed (km/h)	Acceleration Amplitude RMS			Gap between Acceleration Amplitude RMS	
	80	100	120	80 to 100	100 to 120
Standard tunnel	$6.23 \times 10^{-4}$	$1.02 \times 10^{-3}$	$5.88 \times 10^{-4}$	$3.97 \times 10^{-4}$	$4.32 \times 10^{-4}$
Tunnel With CFRP rebar Ø12	$4.85 \times 10^{-4}$	$8.68 \times 10^{-4}$	$5.57 \times 10^{-4}$	$3.83 \times 10^{-4}$	$3.11 \times 10^{-4}$

#### Analysis at a Point on the Ground Surface 40 m from the Tunnel (Point B)

Figure 21 shows the amplitude spectral curves of acceleration at 40 m from the tunnel center at various subway speeds. As can be seen, the acceleration amplitude at a large distance from the tunnel center (point A) is small, with the peaks of the acceleration amplitude occurring in a single periodic cycle. However, the peaks of the acceleration amplitude increase as the speed of the subway train increases. No amplification dynamics are observed in the speed range used for the study, but the acceleration amplitude RMS increases significantly when the subway train reaches 100 km/h (Figure 22).

A slight reduction in acceleration amplitude is observed when the tunnel is reinforced with Ø12 CFRP reinforcement bars. When the metro train travels at 60, 80, and 100 km/h, the acceleration amplitude RMS is  $9.312 \times 10^{-5}$  m/s<sup>2</sup>/Hz,  $1.190 \times 10^{-4}$  m/s<sup>2</sup>/Hz, and  $2.048 \times 10^{-4}$  m/s<sup>2</sup>/Hz for the standard structure, respectively. For the reinforced structure, the acceleration amplitude RMS is  $9.180 \times 10^{-5}$  m/s<sup>2</sup>/Hz,  $1.168 \times 10^{-4}$  m/s<sup>2</sup>/Hz, and  $2.003 \times 10^{-4}$  m/s<sup>2</sup>/Hz, respectively, at train speeds of 60, 80, and 100 km/h. Therefore, the reduction in acceleration amplitude is 1.42%, 1.85%, and 2.2% when the subway train speed is 60, 80, and 100 km/h, respectively. It follows that the degree of vibration reduction at a point far from the center of the tunnel increases as the speed of the subway increases.

Therefore, the reinforcement of the tunnel with CFRP can contribute to the damping of vibrations in the surrounding buildings by reducing the ground vibrations caused by the passage of the metro train in the tunnel.

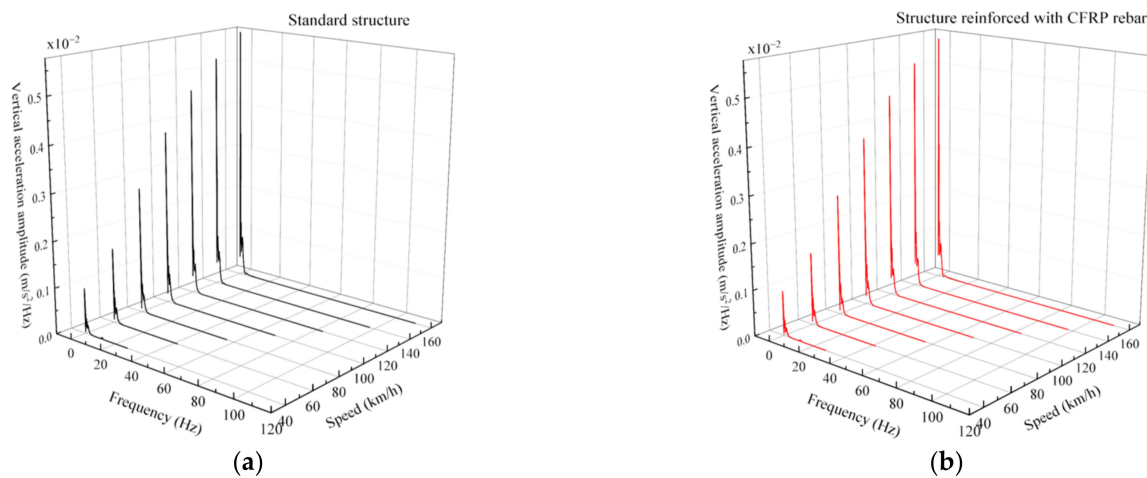


**Figure 21.** Spectrum of the vibration amplitude at point B. (a) Acceleration amplitude-frequency for the standard structure; (b) acceleration amplitude-frequency for the structure reinforced with CFRP rebars.

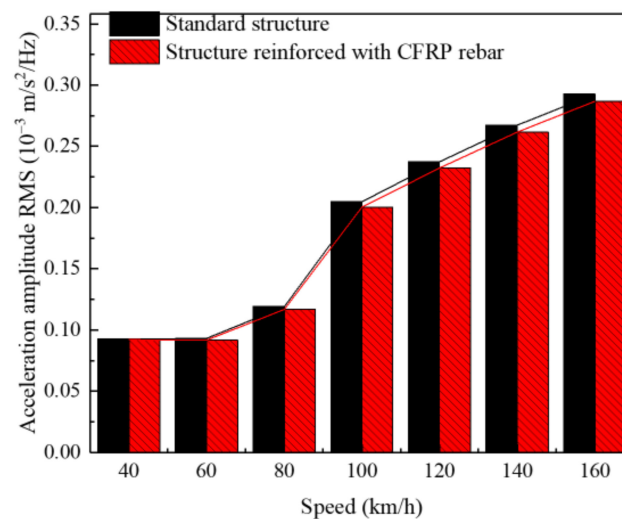


**Figure 22.** Acceleration amplitude RMS diagram at point B.

## 6. Statistical Analysis of CFRP Performance on Soil Dynamic Response

### 6.1. Experimental Setup

The vibrations caused by a moving train become weaker with the increasing distance. Nevertheless, the surrounding buildings are affected by the vibrations while the subway train is moving. In this section, the performance of CFRP in reducing the ground vibration at short and long distances from the tunnel is investigated. Therefore, the influence of some categorical factors (as described in Table 7) and their interaction on the reduction rate of ground vibration due to the travel of the metro train is investigated. The various types of CFRP used are listed in Table 5. At the end of this investigation, a simple and reliable prediction model was proposed.

**Table 7.** Factor and level selected in this analysis.

Parameter Factors	Unit	Code	Level		
			1	2	3
CFRP content (bar diameter)	mm	A	Ø10	Ø12	Ø14
CFRP type	-	B	PNCHS	PNCHM	PCHM
Distance from tunnel center	m	C	0	11	40
Response variable	Reduction rate of the ground-borne vibration				

PNCHS: Polyacrylic nitril carbon high strength; PNCHM: Polyacrylic nitril carbon high modulus; PCHM: Pitch carbon high modulus.

For this purpose, Minitab software was used to analyze the ground vibrations when the tunnel is reinforced with CFRP rebars by applying an analysis of variance to the designed orthogonal array [45]. A full fractional factorial design was used, mainly the standard L27 ( $3^{13-10}$ ) orthogonal array. The orthogonal array consisted of three factors at three levels with 27 runs, which was chosen for its ability to fully capture the interaction between the independent variables [46]. Three levels were defined for each factor, as shown in Table 7. The first row (A) is associated with the CFRP content defined by the bar diameter, the second row (B) indicates the type of CFRP used, and the third row (C) represents the distance from the tunnel center (point A). The three levels of each factor are defined by “1, 2 or 3” in the standard orthogonal arrangement L27 ( $3^{13-10}$ ) [47,48]. In this way, the ground vibration reduction rate defined in Equation (11) was determined from the calculated data for each numerical model run. The data were selected randomly to ensure that the model met certain statistical assumptions and to minimize the effects of factors not included in the experimental design.

$$r_{GV} = \left(1 - \frac{D_{\text{withCFRP}}}{D_{\text{standard}}}\right) \times 100 \quad (11)$$

where  $D_{\text{withCFRP}}$  is the ground acceleration amplitude RMS when the tunnel lining concrete is reinforced with CFRP rebar and  $D_{\text{standard}}$  is the ground acceleration amplitude RMS for the standard tunnel.

## 6.2. Analysis of Factors Influencing the Reduction Rate of Ground Vibrations

The analysis of variance consists of various variables, which are described as follows:

- the degrees of freedom (DF), which correspond to the information content of the experimental design;
- adjusted sums of squares (Adj SS), which correspond to the measures of variation for the different components of the experimental design;
- adjusted mean squares (Adj MS), which measure the proportion of variation explained by a term or experimental design;
- sequential sums of squares (Seq SS), which correspond to measures of variation for different components of the experimental design;
- contribution, which indicates the percentage contribution of each source in the table ANOVA under Sequential Sums of Squares Total (Seq SS);
- F-value, which appears for each term in the analysis of variance table; and
- $p$ -Value is a probability that measures the evidence against the null hypothesis.

The variables, all of which are related, contribute to the definition of the  $p$ -value. Further details on the methods, principles, and formulas related to the statistical index used in the present study can be found in [49]. The analysis of variance presented in Tables 8 and 9 show that all terms in the linear and two-way interaction models had a  $p$ -value below the 5% significance level ( $\beta = 0.05$ ).

**Table 8.** Analysis of variance for speed of 100 km/h.

Source	DF	Seq SS	Contribution	Adj SS	Adj MS	F-Value	p-Value
Model	18	1231.56	98.30%	1231.56	68.420	25.68	0.000
Linear	6	962.67	76.84%	962.67	160.446	60.23	0.000
CFRP content	2	106.44	8.50%	106.44	53.219	19.98	0.001
CFRP type	2	147.88	11.8%	147.88	73.941	27.76	0.000
Distance from tunnel center	2	708.35	56.34%	708.35	354.177	132.95	0.000
Two-way interactions	12	268.88	21.46%	268.88	22.407	8.41	0.003
CFRP content * CFRP type	4	18.47	1.47%	18.47	4.617	1.73	0.235
CFRP bar * Distance from tunnel center	4	111.09	8.87%	111.09	27.772	10.43	0.003
CFRP type * Distance from tunnel center	4	139.32	11.12%	139.32	34.831	13.06	0.001
Error	8	21.31	1.70%	21.31	2.664		
Total	26	1252.87	100%				

“\*” define the coupling of two variables.

**Table 9.** Analysis of variance for speed of 60 km/h.

Source	DF	Seq SS	Contribution	Adj SS	Adj MS	F-Value	p-Value
Model	18	2022.26	99.81%	2022.26	112.348	204.68	0.000
Linear	6	1848.41	91.23%	1712.08	285.347	519.85	0.000
CFRP content	2	48.58	2.40%	46.66	23.329	42.50	0.000
CFRP type	2	172.53	8.52%	109.19	54.597	99.47	0.000
Distance from tunnel center	2	1627.30	80.32%	1321.98	660.988	1204.21	0.000
Two-way interactions	12	173.85	8.58%	173.85	14.487	26.39	0.000
CFRP content * CFRP type	4	11.67	0.58%	3.69	0.923	1.68	0.257
CFRP content * Distance from tunnel center	4	59.45	2.93%	49.09	12.273	22.36	0.000
CFRP type * Distance from tunnel center	4	102.73	5.07%	102.73	25.684	46.79	0.000
Error	7	3.84	0.19%	3.84	0.549		
Total	25	2026.10	100%				

“\*” define the coupling of two variables.

The results of the analysis of variance presented in Tables 8 and 9 for the speeds of 100 and 60 km/h, respectively, show that all three factors of the linear model have a  $p$ -value of less than 5%, and thus have a very significant influence on the distribution of the ground vibration characteristics. For the two-way interaction model, the analysis shows that the  $p$ -value of the interaction effect between the CFRP content and the CFRP type is greater than 5%, and thus insignificant for the reduction in ground vibrations.

The main effect and interaction diagrams of the studied factors affecting ground vibrations are shown in Figures 23 and 24. Only analyses with a significant  $p$ -value are considered in this section.

In the mean effect plots in Figure 23a–c, each point represents the mean rate of reduction in ground vibrations for a corresponding factor. The horizontal reference lines indicate the mean response for all test series. If the points of a particular factor connected by a line are close to the horizontal reference line, the factor influence is insignificant. On the other hand, the steeper the line connecting a factor point, the greater its influence. As can be seen from the diagram of the mean values, the mean values of the responses differ from one factor to another, although the shape of the curve for the speeds of 60 and 100 km/h is almost identical.

Moreover, the influence of distance (distance between the tunnel and the calculation point) on the distribution of vibration characteristics is dominant due to the steep slope of the line connecting the points (Figure 23c). Therefore, the distance greatly influences the reduction rate of ground vibrations. However, it is observed that the performance of the CFRP reinforcements increases depending on the type or diameter of the bar used (Figure 23a,b).

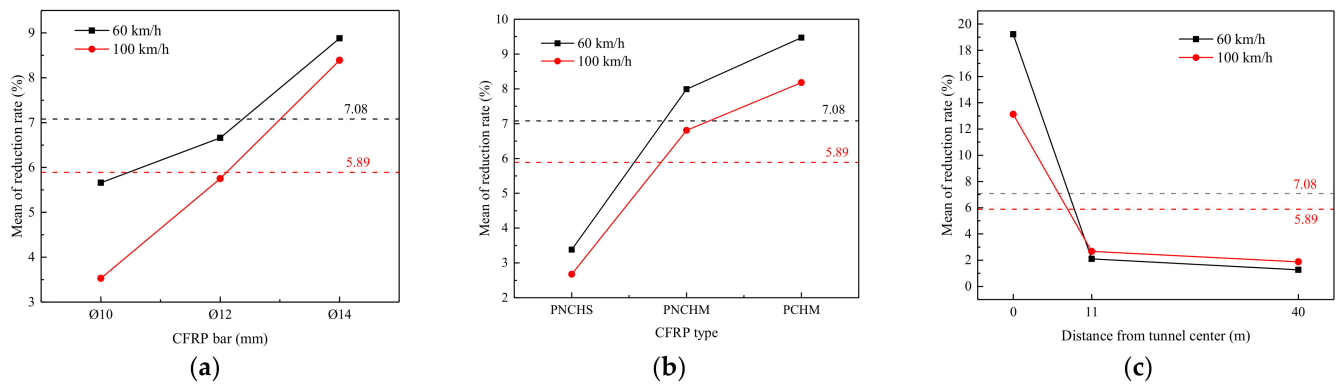


**Figure 23.** Reduction rate for each selected factor. (a) CFRP content; (b) CFRP type; (c) distance from the tunnel center.

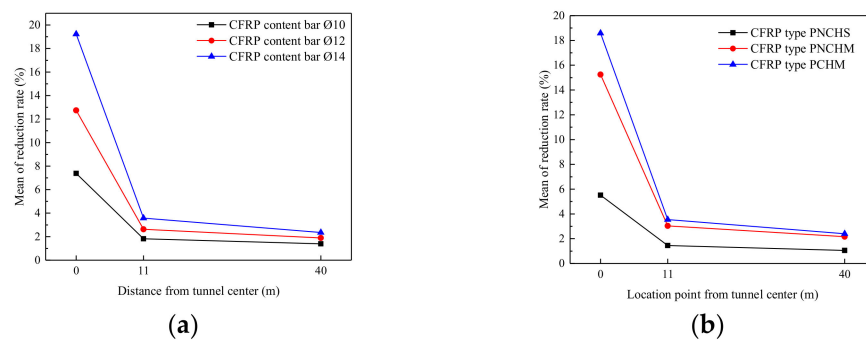


**Figure 24.** Interaction plot matrix of the reduction rate of the ground vibration at the speed of 100 km/h. (a) CFRP content \* Distance; (b) CFRP Type \* Distance.

Figure 24a,b shows the average response of CFRP reinforcement's influence on the soil's dynamic response during the passage of a subway train at 100 km/h in the tunnel. In this section, the degree of vibration reduction at the ground surface was analyzed considering the interaction between the CFRP bar used and the distance. The interaction diagrams confirm the analysis performed above. The degree of vibration reduction is very large at 0 m, regardless of the content and type of CFRP, and decreases drastically at 40 m distance from the tunnel. The vibration reduction rate at the ground surface strongly depends on the proximity to the tunnel. Near the tunnel, the vibration reduction rate is very high and decreases drastically with the increasing distance from the tunnel. Therefore, the distance has a significant influence on the performance of the CFRP reinforcement.

To better assess the effects of each factor studied, a Pareto diagram of the standardized effect at a speed of 100 km/h was also created (see Figure 25). In this Pareto diagram, the bars representing factors C, B, A, BC, and AC cross the reference line 2.31. These factors are statistically significant at the 0.05 level with the terms of the presented model. According to the magnitude of each term described in the Pareto diagram, the distance between the calculation points and the tunnel significantly influences the reduction in ground vibrations. Since the objective of this section is to study the performance of CFRP reinforcement, the factor "CFRP type" contributes more to the reduction in ground vibration than the factor "CFRP content". As can be seen from the Pareto diagram, the BC term is larger than the AC term, indicating that the CFRP type factor is influential over a large distance from the tunnel.

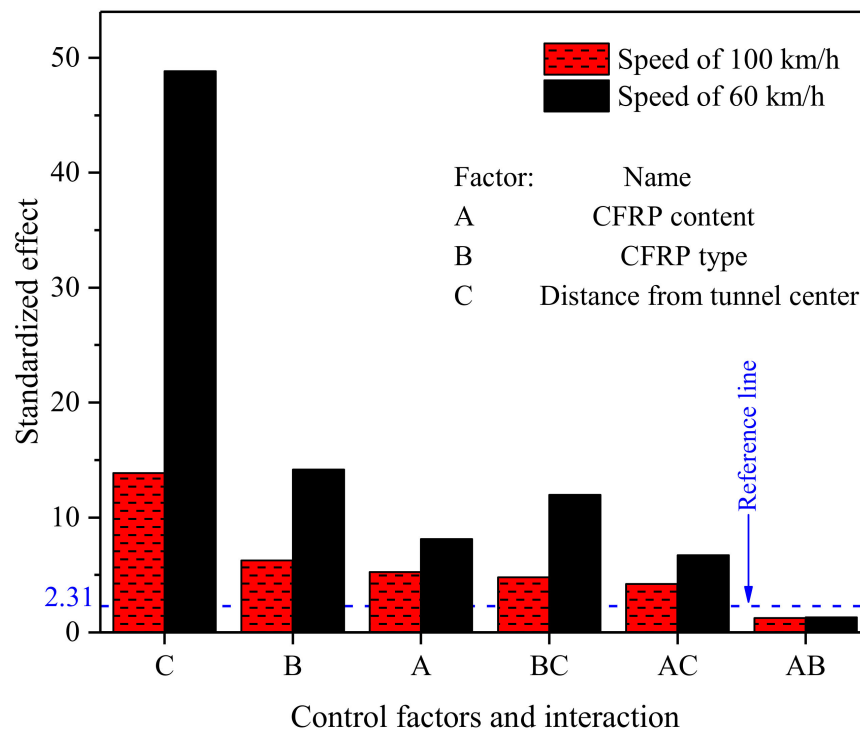


**Figure 25.** Pareto diagram of the standardized effect for vibration propagation reduction.

Spacing has a significant impact on the effect of CFRP in reducing ground vibration. CFRP reinforcement is most effective in the area of load application. Nevertheless, a slight reduction is observed at a distance far from the tunnel. According to the statistical analyses, the factor “CFRP content” in the tunnel lining has a more negligible influence on the reduction in ground vibrations than the factor “CFRP type”. According to the Pareto diagram and the variance analysis table, the combination of both factors has very little influence on the vibration reduction rate. Therefore, the combination of the two factors in a tunnel structure would be a loss. It is recommended to give priority to the “CFRP type” factor. Therefore, CFRP reinforcement with high stiffness is better. However, if it is difficult to find CFRP with high stiffness, the second factor “CFRP content” can be considered.

### 6.3. A Predictive Model of the Vibration Propagation Reduction at the Ground Surface

To determine the dynamic response of the ground surface independent of the reinforcement properties (CFRP type and CFRP content) and the distance from the tunnel center, the relationship between the reduction rate of ground vibration and the above factors was established using the multiple linear regression equation (Equation (12)) shown below. In establishing the equation, the interaction CFRP-type CFRP-content term, which is statistically insignificant, was excluded.

$$y = \chi + \delta_1 Z_1 + \delta_2 Z_2 + \dots + \delta_k Z_k \quad (12)$$

where  $y$  represents the dependent or response variable (ground vibration reduction rate);  $\chi$  intercept is the response value when all the independent variables are zero;  $\delta_1, \delta_2, \dots, \delta_k$  represent coefficients or parameters, which reflect the contributions of each predictor in predicting the response;  $Z_1, Z_2, \dots, Z_k$  are independent variables or values of the influential factors and their coupling.

A multivariate regression analysis was performed individually for the train traveling at different speeds to create a specific predictive model to accurately estimate the dynamic response of the soil with the CFRP reinforcement according to the previously defined orthogonal arrangement. The prediction models were developed for a tunnel buried in soft soil with the subway train traveling at 60 and 100 km/h. The regression

parameters provided a reasonably accurate estimate of the ground vibration reduction rate, which is shown in Table 10 following Equation (12). In this table,  $y_{RGV}$  is the ground vibration reduction rate, and the influencing factors are specifically the CFRP content, the CFRP type, and the distance from the tunnel center. The CFRP content distance and the CFRP type distance are respectively denoted as  $C_{RGV}$ ,  $T_{RGV}$ ,  $D_{RGV}$ ,  $C_{RGV}D_{RGV}$ , and  $T_{RGV}D_{RGV}$ . As for the CFRP type, only the elastic modulus was considered in the calculations. The standard errors (SE) of each estimated parameter were also presented, along with their 95% confidence interval (CI). From the general factor regression analysis, all the prediction models had regression coefficients ( $R^2$ ) close to 0.983, which indicates that these equations have a relatively high degree of fit. Therefore, the reduction rate of the vibration at the ground surface according to the CFRP material can be calculated by these formulations.

**Table 10.** Summary of prediction model.

Prediction Model for Reduction Rate of the Vibration at the Ground Upper Surface						
$y_{RGV} = \chi + \delta_1 C_{RSD} + \delta_2 T_{RGV} + \delta_3 D_{RGV} + \delta_4 C_{RGV}D_{RGV} + \delta_5 T_{RGV}D_{RGV}$						
Parameter	$\chi$	$\delta_1$	$\delta_2$	$\delta_3$	$\delta_4$	$\delta_5$
			Train speed of 100 km/h			
Estimate	−27.2	2.160	0.02439	0.714	−0.0556	−0.000607
SE Estimate	10.0	0.777	0.00762	0.419	0.0324	0.000318
95% CI	(−48.1, −6.4)	(0.545, 3.775)	(0.00853, 0.04024)	(−0.156, 1.584)	(−0.1230, 0.0118)	(−0.001269, 0.000055)
			Train speed of 60 km/h			
Estimate	−15.2	1.44	0.0241	0.396	−0.0376	−0.000633
SE Estimate	13.6	1.05	0.0103	0.568	0.0440	0.000432
95% CI	(−43.5, 13.0)	(−0.75, 3.63)	(0.0026, 0.0457)	(−0.785, 1.576)	(−0.1291, 0.0538)	(−0.001531, 0.000265)

## 7. Conclusions

Ground vibrations caused by the operation of a subway train in a tunnel were investigated by implementing a nonlinear 3D finite element model in Abaqus software [25]. The reliability of the numerical model, which was developed in accordance with the dimensions and conditions of the Shanghai subway section, was verified by comparing the simulation results with field test data from previous work. The load of the subway wheels was integrated into the numerical model as a transient moving load via a subroutine DLOAD developed in Fortran. Once the created model was successfully validated after calibrations, the ground vibrations during the operation in a tunnel reinforced with CFRP bars were investigated, and a series of parameter studies were performed. In addition, statistical analyses were performed to investigate the relationship between the dynamic response of the soil in a tunnel lining reinforced with CFRP bars and influencing factors, such as the CFRP bars used, the CFRP type, and the location of the calculation point. Finally, a prediction model for the dynamic response of the soil in a tunnel lining reinforced with CFRP bars was proposed. The following conclusions were drawn from this study:

- The developed 3D FE model was suitable for accurately simulating the dynamic behavior of the soil during the subway operation in a tunnel, since the error calculated by the comparative analysis was small.
- The effects of two subway trains running simultaneously in the downward and upward directions should be taken into account in the design of buildings in the vicinity of the subway line since the crossing of subway trains is unpredictable, while the vibrations generated by these two subway trains are almost twice as high as those generated by a single subway train.
- Reinforcing the concrete of the tunnel lining with CFRP rebars increases the dynamic capacity of the soil to respond to the loads caused by the passage of a subway train in a tunnel. A reduction in vibration is observed at the surface of the soil as well as at a depth of the soil, with the rate of reduction varying from one point to another. Therefore, reinforcing the tunnel lining with CFRP bars mitigates to some extent the discomfort experienced by surrounding buildings during the subway operation.

- The analysis of the effect of the subway's travel speed on the ground vibration shows that the maximum peak of the vibration amplitude increases with speed. After calculating the vibration amplitude RMS in the frequency domain, dynamic amplification was observed at the ground surface above the tunnel when the speed of the subway train reached 100 km/h. The dynamic amplification disappears with the increasing distance from the tunnel. Nevertheless, the difference between the vibration amplitude RMS at speeds from 80 to 100 km/h is huge. The speed of 100 km/h, which coincides with the shear wave velocity of a soil layer, illustrates the influence of the system mechanical properties on the soil's dynamic response.
- The reinforcement of the tunnel with CFRP bars reduces vibrations in the ground regardless of the operating speed of the subway. In general, the reduction rate increases as the speed of the metro train increases. The effect of CFRP bars in the structure decreases when the train reaches the critical speed, which coincides with the shear wave velocity of a soil layer. Nevertheless, the vibrations are less amplified when the distance between the dynamic acceleration and the speed of the subway train decreases from 80 to 120 km/h.

In addition, a statistical analysis of the dynamic response of the soil was performed when the tunnel lining is reinforced with CFRP bars, considering three factors (CFRP rod diameter, CFRP type, and distance from the tunnel center). The following results were obtained:

- The distance has a significant impact on the effect of CFRP reinforcement in reducing ground vibration. According to the results, the CFRP reinforcement is more effective near the tunnel. According to the statistical analyses, the factor "CFRP content" in the tunnel lining has a more negligible influence on the reduction in ground vibration than the factor "CFRP type". The combination of the two factors has little influence on the vibration reduction rate. Therefore, it would be a waste to combine the effect of both factors in a tunnel design. As a result, the use of a CFRP reinforcement with high stiffness is recommended. However, if it is difficult to find CFRP with high stiffness, the CFRP content in the tunnel lining can be considered.
- The proposed multiple linear regression model predicted with reasonable accuracy the reduction in ground vibration as a function of the type and content of CFRP used at any distance from the tunnel center buried in a soft deposit.

**Author Contributions:** Conceptualization, I.V.L.C. and J.C.; methodology, I.V.L.C. and J.C.; software, I.V.L.C.; validation, I.V.L.C. and J.C.; formal analysis, I.V.L.C. and J.C.; investigation, I.V.L.C. and J.C.; resources, J.C.; data curation, I.V.L.C. and J.C.; writing—original draft preparation, I.V.L.C.; writing—review and editing, I.V.L.C. and J.C.; visualization, I.V.L.C.; supervision, J.C.; project administration, J.C.; funding acquisition, J.C. All authors have read and agreed to the published version of the manuscript.

**Funding:** This research was funded by the National Natural Science Foundation of China (Grant No. 52178151); Shanghai TCM Chronic Disease Prevention and Health Service Innovation Center (Grant No. ZYJKFW201811009); and State Key Laboratory for Disaster Reduction of Civil Engineering (Grant No. SLDRCE19-B-22).

**Data Availability Statement:** Not applicable.

**Acknowledgments:** The authors acknowledge the support from the National Natural Science Foundation of China; Shanghai TCM Chronic Disease Prevention and Health Service Innovation Center; and State Key Laboratory for Disaster Reduction of Civil Engineering.

**Conflicts of Interest:** The authors declare no conflict of interest.

## Appendix A

**Table A1.** Natural frequency obtained from the modal analysis (cycle/second).

Mode	Frequency	Mode	Frequency	Mode	Frequency	Mode	Frequency
1	2.75497	14	3.00939	27	3.06791	40	3.141291
2	2.75498	15	3.01641	28	3.07973	41	3.15007
3	2.86599	16	3.01931	29	3.08658	42	3.15021
4	2.86510	17	3.02062	30	3.08669	43	3.15334
5	2.98193	18	3.03278	31	3.09806	44	3.15411
6	2.98341	19	3.03346	32	3.10431	45	3.16050
7	2.98193	20	3.03457	33	3.10664	46	3.16303
8	2.98193	21	3.04378	34	3.10670	47	3.16306
9	2.98742	22	3.04887	35	3.10746	48	3.16457
10	2.99916	23	3.04978	36	3.11628	49	3.16610
11	3.00061	24	3.05046	37	3.11866	50	3.16624
12	3.00172	25	3.05361	38	3.12790		
13	3.00194	26	3.06765	39	3.12791		

## References

- Xia, H.; Cao, Y. Problem of railway traffic induced vibrations of environments. *J. Railw. Sci. Eng.* **2004**, *1*, 44–51.
- Guo, T.; Cao, Z.; Zhang, Z.; Li, A. Numerical simulation of floor vibrations of a metro depot under moving subway trains. *J. Vib. Control* **2018**, *24*, 4353–4366. [\[CrossRef\]](#)
- Lopes, P.; Ruiz, J.F.; Costa, P.A.; Rodríguez, L.M.; Cardoso, A.S. Vibrations inside buildings due to subway railway traffic. Experimental validation of a comprehensive prediction model. *Sci. Total Environ.* **2016**, *568*, 1333–1343. [\[PubMed\]](#)
- Connolly, D.P.; Marecki, G.P.; Kouroussis, G.; Thalassinakis, I.; Woodward, P.K. The growth of railway ground vibration problems—A review. *Sci. Total Environ.* **2016**, *568*, 1276–1282. [\[CrossRef\]](#) [\[PubMed\]](#)
- López-Mendoza, D.; Romero, A.; Connolly, D.P.; Galvín, P. Scoping assessment of building vibration induced by railway traffic. *Soil Dyn. Earthq. Eng.* **2017**, *93*, 147–161. [\[CrossRef\]](#)
- Lang, J. Ground-borne vibrations caused by trams, and control measures. *J. Sound Vib.* **1988**, *120*, 407–412. [\[CrossRef\]](#)
- Xu, P.; Wu, Y.; Huang, L.; Zhang, K. Study on the Progressive Deterioration of Tunnel Lining Structures in Cold Regions Experiencing Freeze–Thaw Cycles. *Appl. Sci.* **2021**, *11*, 5903. [\[CrossRef\]](#)
- Li, R.; Gao, X.; Kong, C. Study on the aging deterioration curve of tunnel lining in water rich area. In *IOP Conference Series: Materials Science and Engineering*; IOP Publishing: Bristol, UK, 2020.
- Han, W.; Jiang, Y.; Gao, Y.; Koga, D. Study on design of tunnel lining reinforced by combination of pcm shotcrete and FRP grid technique. In *IOP Conference Series: Earth and Environmental Science*; IOP Publishing: Bristol, UK, 2020.
- Jiang, Y.; Wang, X.; Li, B.; Higashi, Y.; Taniguchi, K.; Ishida, K. Estimation of reinforcing effects of FRP-PCM method on degraded tunnel linings. *Soils Found.* **2017**, *57*, 327–340. [\[CrossRef\]](#)
- Hollaway, L. A review of the present and future utilisation of FRP composites in the civil infrastructure with reference to their important in-service properties. *Constr. Build. Mater.* **2010**, *24*, 2419–2445. [\[CrossRef\]](#)
- Weaver, A. Composites: World markets and opportunities. *Mater. Today* **1999**, *2*, 3–6. [\[CrossRef\]](#)
- Han, W.; Jiang, Y.; Zhang, X.; Koga, D.; Gao, Y. Quantitative assessment on the reinforcing behavior of the CFRP-PCM method on tunnel linings. *Geomech. Eng.* **2021**, *25*, 123–134.
- Li, W.; Gang, W.; Dong, Z.; Wang, S. Experimental study on a pre-damaged scaled tunnel model strengthened with CFRP grids. *J. Southeast Univ.* **2017**, *33*, 196–202.
- Dolan, C.W. FRP Prestressing in the USA. *Concr. Int.* **1999**, *21*, 21–24.
- Fukuyama, H. FRP composites in Japan. *Concr. Int.* **1999**, *21*, 29–32.
- Bakis, C.E.; Bank, L.C.; Brown, V.; Cosenza, E.; Davalos, J.; Lesko, J.; Machida, A.; Rizkalla, S.; Triantafillou, T. Fiber-reinforced polymer composites for construction-state-of-the-art review. *J. Compos. Constr.* **2002**, *6*, 73–87. [\[CrossRef\]](#)
- Caratelli, A.; Meda, A.; Rinaldi, Z.; Spagnuolo, S. Precast tunnel segments with GFRP reinforcement. *Tunn. Undergr. Space Technol.* **2016**, *60*, 10–20. [\[CrossRef\]](#)
- Laníková, I.; Stepanek, P.; Venclovský, J. Optimization of a tunnel lining reinforced with FRP. In *Key Engineering Materials*; Trans Tech Publication: Zurich, Switzerland, 2016.
- Caratelli, A.; Meda, A.; Rinaldi, Z.; Spagnuolo, S.; Maddaluno, G. Optimization of GFRP reinforcement in precast segments for metro tunnel lining. *Compos. Struct.* **2017**, *181*, 336–346. [\[CrossRef\]](#)
- Spagnuolo, S.; Meda, A.; Rinaldi, Z.; Nanni, A. Curvilinear GFRP bars for tunnel segments applications. *Compos. Part B Eng.* **2018**, *141*, 137–147. [\[CrossRef\]](#)
- Zhao, C.; Tang, Z.; Wang, P.; Feng, J.; Zhou, J.; Kong, X.; Geng, H.; Jin, F.; Fan, H. Blast responses of shallow-buried prefabricated modular concrete tunnels reinforced by BFRP-steel bars. *Undergr. Space* **2022**, *7*, 184–198. [\[CrossRef\]](#)

23. Abbood, I.S.; Aldeen Odaa, S.; Hasan, K.F.; Jasim, M.A. Properties evaluation of fiber reinforced polymers and their constituent materials used in structures—A review. *Mater. Today Proc.* **2021**, *43*, 1003–1008.
24. Karsli, N.G.; Ozkan, C.; Aytac, A.; Deniz, V. Effects of sizing materials on the properties of carbon fiber-reinforced polyamide 6, 6 composites. *Polym. Compos.* **2013**, *34*, 1583–1590. [[CrossRef](#)]
25. Abaqus, F. *Dassault Systemes Simulia Corporation; FEA Abaqus*: Providence, RI, USA, 2014.
26. Bathe, K.-J. *Finite Element Procedures*; Prentice Hall: Upper Saddle River, NJ, USA, 2006.
27. Lee, I.-W.; Kim, D.-O.; Jung, G.-H. Natural frequency and mode shape sensitivities of damped systems: Part I, distinct natural frequencies. *J. Sound Vib.* **1999**, *223*, 399–412. [[CrossRef](#)]
28. Zhai, W.; Xia, H.; Cai, C.; Gao, M.; Li, X.; Guo, X.; Zhang, N.; Wang, K. High-speed train-track-bridge dynamic interactions—Part I: Theoretical model and numerical simulation. *Int. J. Rail Transp.* **2013**, *1*, 3–24. [[CrossRef](#)]
29. Chango, I.V.L.; Assogba, O.C.; Yan, M. Estimating static and dynamic stress distribution in a railway embankment reinforced by geogrid and supported by pile system. *Transp. Infrastruct. Geotechnol.* **2022**, *2022*, 1–28. [[CrossRef](#)]
30. Assogba, O.C.; Sun, Z.; Tan, Y.; Nonde, L.; Bin, Z. Finite-element simulation of instrumented asphalt pavement response under moving vehicular load. *Int. J. Geomech.* **2020**, *20*, 04020006. [[CrossRef](#)]
31. Zienkiewicz, O.C.; Taylor, R.L.; Zhu, J.Z. *The Finite Element Method: Its Basis and Fundamentals*; Elsevier: Amsterdam, The Netherlands, 2005.
32. Li, S.; Guo, Z.; Yang, Y. Dynamic viscoelastic response of an instrumented asphalt pavement under various axles with non-uniform stress distribution. *Road Mater. Pavement Des.* **2016**, *17*, 446–465. [[CrossRef](#)]
33. Chango, I.V.L.; Assogba, G.C.; Yan, M.; Xianzhang, L.; Mitobaba, J.G. Impact Assessment of Asphalt Concrete in Geogrid-Reinforced-Pile-Supported Embankment During High-Speed Train Traffic. *Balt. J. Road Bridge Eng.* **2022**, *17*, 135–163. [[CrossRef](#)]
34. Huang, Z.-K.; Pitolakis, K.; Tsinidis, G.; Argyroudis, S.; Zhang, D.-M. Seismic vulnerability of circular tunnels in soft soil deposits: The case of Shanghai metropolitan system. *Tunn. Undergr. Space Technol.* **2020**, *98*, 103341. [[CrossRef](#)]
35. Huang, Q.; Li, P.; Zhang, D.; Huang, H.; Zhang, F. Field Measurement and Numerical Simulation of Train-Induced Vibration from a Metro Tunnel in Soft Deposits. *Adv. Civ. Eng.* **2021**, *2021*, 6688746. [[CrossRef](#)]
36. Yang, L.; Wang, G.; Liu, Q.; Lei, G. A study on the dynamic properties of soft soil in Shanghai. In *Soil and Rock Behavior and Modeling*; American Society of Civil Engineers: Reston, VA, USA, 2006; pp. 466–473.
37. Zhang, D.-M.; Huang, Z.-K.; Wang, R.-L.; Yan, J.-Y.; Zhang, J. Grouting-based treatment of tunnel settlement: Practice in Shanghai. *Tunn. Undergr. Space Technol.* **2018**, *80*, 181–196. [[CrossRef](#)]
38. Oreste, P. Analysis of structural interaction in tunnels using the convergence–confinement approach. *Tunn. Undergr. Space Technol.* **2003**, *18*, 347–363. [[CrossRef](#)]
39. Michał, S.; Andrzej, W. Calibration of the CDP model parameters in Abaqus. In Proceedings of the 2015 World Congress on Advances in Structural Engineering and Mechanics (ASEM15), Incheon, Korea, 7 September 2015.
40. Chango, I.V.L.; Yan, M.; Ling, X.; Liang, T.; Assogba, O.C. Dynamic Response Analysis of Geogrid Reinforced Embankment Supported by CFG Pile Structure During a High-Speed Train Operation. *Lat. Am. J. Solids Struct.* **2019**, *16*. [[CrossRef](#)]
41. Gao, J.; Zhai, W. Dynamic effect and safety limits of rail weld irregularity on high-speed railways. *Sci. Sin. Technol.* **2014**, *44*, 697–706.
42. Bian, X.; Jiang, H.; Chang, C.; Hu, J.; Chen, Y. Track and ground vibrations generated by high-speed train running on ballastless railway with excitation of vertical track irregularities. *Soil Dyn. Earthq. Eng.* **2015**, *76*, 29–43. [[CrossRef](#)]
43. Zhou, S. *Dynamics of Rail Transit Tunnel Systems*; Academic Press: Cambridge, MA, USA, 2019.
44. Spagnuolo, S.; Meda, A.; Rinaldi, Z.; Nanni, A. Precast concrete tunnel segments with GFRP reinforcement. *J. Compos. Constr.* **2017**, *21*, 04017020. [[CrossRef](#)]
45. Tanaydin, S. *Robust Design and Analysis for Quality Engineering*; Taylor & Francis: Abingdon, UK, 1998.
46. Ghani, J.A.; Choudhury, I.; Hassan, H. Application of Taguchi method in the optimization of end milling parameters. *J. Mater. Process. Technol.* **2004**, *145*, 84–92. [[CrossRef](#)]
47. Assogba, O.C.; Tan, Y.; Dong, W.; Lv, H.; Anato, N.J. Field evaluation and statistical analysis of the dynamic response of semi-rigid pavement under full-scale moving truck load. *Road Mater. Pavement Des.* **2021**, *2021*, 1–29. [[CrossRef](#)]
48. Anato, N.J.; Assogba, O.C.; Tang, A.; Diakité, Y.; Cho Mya, D. Numerical and statistical investigation of the performance of closed-cell aluminium foam as a seismic isolation layer for tunnel linings. *Eur. J. Environ. Civ. Eng.* **2021**, 1–25. [[CrossRef](#)]
49. Bryman, A.; Cramer, D. *Quantitative Data Analysis with Minitab: A Guide for Social Scientists*; Routledge: Oxfordshire, UK, 2003.